Bachelor Project

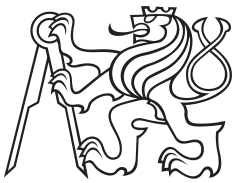

Czech Technical University in Prague

F3

Faculty of Electrical Engineering
Department of Control Engineering

Alternative methods of eVTOL vehicles stabilization

Adam Pelech

Supervisor: Doc. Ing. Martin Hromčík, Ph.D.
Field of study: Cybernetics and Robotics
May 2024

BACHELOR‘S THESIS ASSIGNMENT

I. Personal and study details

Student's name: **Pelech Adam** Personal ID number: **507263**

Faculty / Institute: **Faculty of Electrical Engineering**

Department / Institute: **Department of Control Engineering**

Study program: **Cybernetics and Robotics**

II. Bachelor’s thesis details

Bachelor’s thesis title in English:

Alternative methods of eVTOL vehicles stabilization

Bachelor’s thesis title in Czech:

Alternativní způsoby stabilizace eVTOL prostředků

Guidelines:

The thesis will consist of the study of alternative methods of eVTOL vehicle stabilization.
The goal of the thesis is analysis of behaviour of eVTOL vehicles during vertical takeoff and landing in the relation to the characteristics of the method of stabilization and during the effect of external atmospheric factors.
The motivation is formulation of minimal criteria for the characteristics of the stabilization elements and comparison of their results with results of realistic simulation scenarios.
Instructions:
1) Study the mechanics of eVTOL vehicles in the hover mode.
2) Formulate the equations for maximum theoretical deviations and settling time in regards to characteristics of stabilization elements and external factors.
3) Create a realistic simulation scenarios containing for example flight dynamics, wind gusts and propeller characteristics.
4) Design a stabilization system using classical methods of control design, compare to theoretical results.
5) Design a stabilization system using modern methods of control design, for example sliding mode, switching or MPC, compare to previous results.

Bibliography / sources:

[1] Roger W. Pratt Johnson Flight Control Systems: Practical Issues in Design and Implementation. Institution of Engineering and Technology, 2000, https://app.knovel.com/kn/resources/kpFCSPIDI2/toc
[2] B. L. Stevens, F. L. Lewise. N. Johnson Aircraft Control and simulation . Third edition, John Wiley & Sons, Inc. 2016 https://ebookcentral.proquest.com/lib/cvut/reader.action?docID=4039442
[3] Franklin, James A.. (2002). Dynamics, Control, and Flying Qualities of V/STOL Aircraft. American Institute of Aeronautics and Astronautics (AIAA).
https://app.knovel.com/kn/resources/kpDCFQVST2/toc
[4] Johnson, Wayne. Rotorcraft Aeromechanics, Cambridge University Press, 2013.
https://ebookcentral.proquest.com/lib/cvut/reader.action?docID=1139714

Name and workplace of bachelor's thesis supervisor:

doc. Ing. Martin Hromčík, Ph.D. Department of Control Engineering FEE

Name and workplace of second bachelor's thesis supervisor or consultant:

Date of bachelor's thesis assignment: **31.01.2024** Deadline for bachelor thesis submission: **24.05.2024**

Assignment valid until:
by the end of summer semester 2024/2025

doc. Ing. Martin Hromčík, Ph.D.	prof. Ing. Michael Šebek, DrSc.	prof. Mgr. Petr Páta, Ph.D.
Supervisor's signature	Head of department's signature	Dean's signature

III. Assignment receipt

The student acknowledges that the bachelor's thesis is an individual work. The student must produce his thesis without the assistance of others, with the exception of provided consultations. Within the bachelor's thesis, the author must state the names of consultants and include a list of references.

.	
Date of assignment receipt	Student's signature

Acknowledgements

I would like to give thanks to doc. Ing. Martin Hromčík, Ph.D. for consulting and guiding me throughout my work on this thesis, especially for his expertise and for sparking my curiosity.

I am also thankful to my family and friends for supporting me during the time I worked on this thesis.

Declaration

I declare, that I completed this submitted work individually, and that I cited all the used literature.

In Prague, 21. May 2024

Abstract

The aim of this bachelor's thesis is to evaluate the possibility of using alternative stabilization methods for eVTOL vehicles. An analytical approach is taken with a simplified scenario, to analyse motion behaviour of eVTOL vehicles in regard to the propulsion characteristics. A realistic hypothetical civilian eVTOL model and realistic scenarios are created with aerodynamic analysis, propulsion dynamics and wind gusts. Various control methods are implemented to stabilize and control the simulated model. The results are evaluated with regard to the propulsion characteristics. The analytical and simulation results are also compared.

Keywords: eVTOL, eVTOL stabilization, eVTOL control, eVTOL modelling

Supervisor: Doc. Ing. Martin Hromčík, Ph.D.

Abstrakt

Cílem této bakalářské práce je vyhodnotit použitelnost alternativních stabilizačních způsobů pro eVTOL prostředky. Je použit analytický přístup se zjednodušeným scénářem k analyzování chování pohybu eVTOL prostředků vzhledem k charakteristikám pohonů. Jsou vytvořeny realistické scénáře a hypotetický realistický model civilního eVTOL prostředku s aerodynamickou analýzou, dynamikou pohonů a větrnými poryvy. Různé metody řízení jsou implementovány k stabilizaci a ovládání simulovaného modelu. Výsledky jsou vyhodnoceny vzhledem k charakteristikám pohonů. Analytické a simulační výsledky jsou také porovnány.

Klíčová slova: eVTOL, eVTOL stabilizace, řízení eVTOL, modelování eVTOL

Překlad názvu: Alternativní způsoby stabilizace eVTOL prostředků

Contents

Figures

Tables

Chapter 1

Introduction

eVTOL vehicles are a class of aircraft that are capable of vertical takeoff and landing and utilize electrical propulsion as the main propulsion system. The structure of a VTOL aircraft can vary from an almost conventional aeroplane with aerodynamic surfaces providing lift during forward flight, through tilt rotor aircraft, to helicopters and quadcopter-like vehicles. Some notable VTOL aircraft are the Harrier, F-35B and V-22 Osprey.

(a) : BAe Harrier II GR9 [Pin08]

(b) : F-35B Lightning II [NTB19]

(c) : V-22 Osprey [52"14]

Figure 1.1: VTOL aircraft examples

Electric propulsion is applicable in the latter three categories, as it takes form of an electric motor and either a propeller, rotor or a ducted fan. It has several benefits, as it is more flexible, responds faster to controls and is overall simpler mechanically. On the other hand, energy storage is a problem, as batteries tend to be heavier than fuel for the same energy density.

A category of particular interest are tilt rotor aircraft, which can use the electric propulsion for vertical lift, as well as operate like fixed-wing aeroplanes in forward flight [Joh13]. They often include some sort of propeller tilting mechanism, that allows to transition between these two configurations. There aren't many successful examples of this VTOL type that are full scale aircraft, the best example of this is the V-22 Osprey. On the other hand, there are numerous projects for civilian eVTOL aircraft, such as the Zuri 2.0 or Joby S4.

(a) : Zuri 2.0 (concept art) [SE] **(b) :** Joby S4 [Hun23]

Figure 1.2: eVTOL aircraft examples

The control of such vehicles is complicated in the VTOL configuration, as the aerodynamic surfaces have barely any effects at low speeds, the propulsion needs to keep the aircraft flying in a stable position, while also being affected by external elements such as wind. For that often additional stabilization methods are used, such as reaction control systems using diverted compressed air from a jet engine, as that is the case with the Harrier and F-35B.

From that a question arises, as to what are the requirements for the propulsion and stabilization systems to keep the vehicle stable in this configuration. Further, what characteristics are beneficial and important for the propulsion to have.

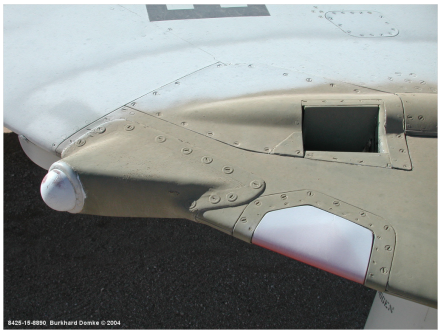

(a) : Reaction control system jet on the wing of the Harrier used for roll control [Dom04]

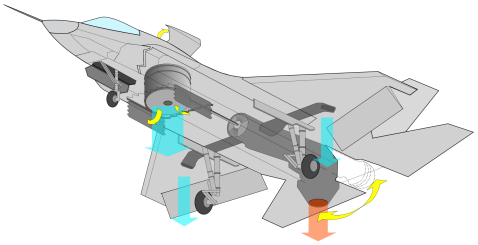

(b) : Schematic of F-35B VTOL configuration ["To08]

Figure 1.3: VTOL aircraft control examples

Objectives

This project's main objective is to evaluate the possibility of using alternative stabilization methods for eVTOL aircraft. Cold gas thrusters are of particular interest, as they are in function similar to reaction control systems used on other VTOL aircraft.

First, simplified analytical equations for eVTOL motion can be formulated, using just the motion laws for a body with six degrees of freedom, disregarding the aerodynamic forces and propulsion dynamics.

Then a realistic model of a hypothetical civilian eVTOL can be created, which could be analysed aerodynamically. Using data from that a simulation model of the modelled aircraft's roll axis can be devised.

Next, a series of classical and modern stabilization controllers can be designed, as well as scenarios to test their response with different propulsion characteristics.

Finally, the simulation results can be evaluated in regard to the propulsion characteristics, and the analytical results can be compared to the realistic simulation results.

Chapter 2

eVTOL behaviour

The motivation behind this chapter is to analytically determine how fixed delay and thrust characteristics of propulsion systems affect the motion capabilities of eVTOL vehicles.

Different motion scenarios are considered, both in terms of translational and rotational motion. Results should consist of minimal rise times achievable or minimal errors and settling times in scenarios with disturbance.

The nature of these results is mostly theoretical, and should be taken as a minimum, since real systems perform differently in many aspects.

2.1 Motion mechanics

The vehicle can be assumed to be a rigid body with six degrees of freedom [Ste15]. To orient the body an axis system is required. An axis system fixed to the body, which is otherwise referred to as the body-axis system [Pra00].

The centre of the axis system is assumed to be located in the centre of mass. When in the steady hover rotation (i.e. $\phi, \theta = 0$), or in other words level with the horizon, the main propulsion elements in the VTOL configuration are oriented upward, creating thrust in the -Z direction. While in hover mode, most aerodynamic forces can be ignored [Fra02].

Axis	Position	Speed	Linear acceleration	Force
Longitudinal	x	u	$\dot{u}$	X
Lateral	y	v	$\dot{v}$	Y
Vertical	z	w	$\dot{w}$	Z
	Angle	Rate	Angular acceleration	Moment
Roll	ϕ	p	$\dot{p}$	L
Pitch	θ	r	$\dot{r}$	M
Yaw	ψ	q	$\dot{q}$	N

Table 2.1: Table of symbols

For later aerodynamic analysis, the wind-axis system is also important. It is for describing the aircraft relative to the airspeeds, and provide the definitions for angle of attack $\alpha = \arctan \frac{w}{u}$ and side-wind angle $\beta = \arctan \frac{v}{u}$.

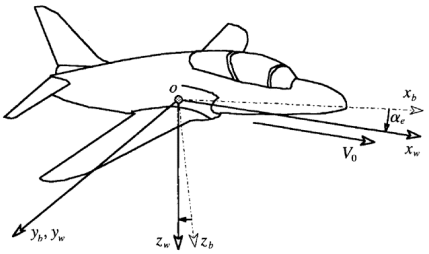

Figure 2.1: Illustration of Body-axis and Wind-axis systems [Pra00]

2.1.1 Angular mechanics

Using Newton's laws of motion following equations can be derived for the roll axis or in principle identical equations can be applied to pitch and yaw axis [Ste15].

$$L(t) = F_L(t) \times l \tag{2.1}$$

$$\dot{p}(t) = \frac{\sum L(t)}{J_x} \tag{2.2}$$

$$p(t) = \int \dot{p}(t)\ dt + p_0 \tag{2.3}$$

$$\phi(t) = \int p(t)\ dt + \phi_0 \tag{2.4}$$

Torque $L(t)[N \cdot m]$ is the cross-product a force $F_L(t)[N]$ acting on the vehicle at a distance $l[m]$ from the roll axis X. The roll acceleration $\dot{p}(t)[\frac{rad}{s^2}]$ is equal to the sum of torques $L(t)$ over the moment of inertia of the roll axis $J_x[\frac{kg}{m^2}]$.

Roll rate $p(t)[\frac{rad}{s}]$ is equal to the integral of the roll acceleration plus the initial condition. Similar equation applies to the roll angle $\phi(t)[rad]$.

Since a rigid body is assumed, and therefore it doesn't deform, it is possible to simplify the acting of some forces on the vehicle. Under the condition that the forces stays constant during a time interval, therefore they all change in steps, then the angular acceleration $\dot{p}$can be simplified to a constant in the respective interval.

$$\dot{p}(t) = \frac{\sum (F_L(t) \times l)}{J_x} \tag{2.5}$$

$$= \frac{\sum ([F_L \cdot i(t)] \times l)}{J_x} \qquad i(t) \ \epsilon \ [-1, 1] \tag{2.6}$$

$$= \dot{p} \qquad \dot{p} \ \epsilon \ [\dot{p}_{max}, \dot{p}_{min}] \tag{2.7}$$

If only propulsion forces are acting, they're dependent on the control input $i[-]$, which can be managed in this way.

2.1.2 Translational mechanics

To describe linear translational motion, Newton's laws of motion are applied to the X, Y and Z axis [Ste15].

$$\dot{u}(t) = \frac{\sum F_x(t)}{m} \tag{2.8}$$

$$u(t) = \int \dot{u}(t) \ dt + u_0 \tag{2.9}$$

$$x(t) = \int u(t) \ dt + x_0 \tag{2.10}$$

The vehicle's linear acceleration $\dot{u}(t)[\frac{m}{s^2}]$ is equal the sum of forces $F_x(t)[N]$ acting on the vehicle in the specified axis. The velocity $u(t)[\frac{m}{s}]$ is the integral of the linear acceleration. Similar applies to the vehicle's position $x(t)[m]$.

There are notable similarities to the angular mechanics in terms of these equations, except for the equations for acceleration. Other than that same principles, including the previous interval restricted simplification to a constant, can be applied to both kinds of motion.

$$\dot{u}(t) = \frac{\sum F_x(t)}{m} \tag{2.11}$$

$$= \frac{\sum F_x \cdot i(t)}{m} \qquad i(t) \ \epsilon \ [-1, 1] \tag{2.12}$$

$$= \dot{u} \qquad \dot{u} \ \epsilon \ [\dot{u}_{max}, \dot{u}_{min}] \tag{2.13}$$

Again, same simplification to a constant can be used as before, further confirming the similarities of translational and rotational motion.

2.2 Reaction to input

2.2.1 Change in rate

The simplest possible scenario, using the roll axis as an example, where an increase or decrease from angular rate p_0 to p is required, can be expressed as following using the motion mechanics.

$$p = \int_{-\infty}^{\infty} \dot{p}\ dt + p_0 \tag{2.14}$$

$$= \int_{-\infty}^{0} 0\ dt + \int_{0}^{T} \dot{p}\ dt + \int_{T}^{\infty} 0\ dt + p_0 \tag{2.15}$$

$$= \Delta p + p_0 \tag{2.16}$$

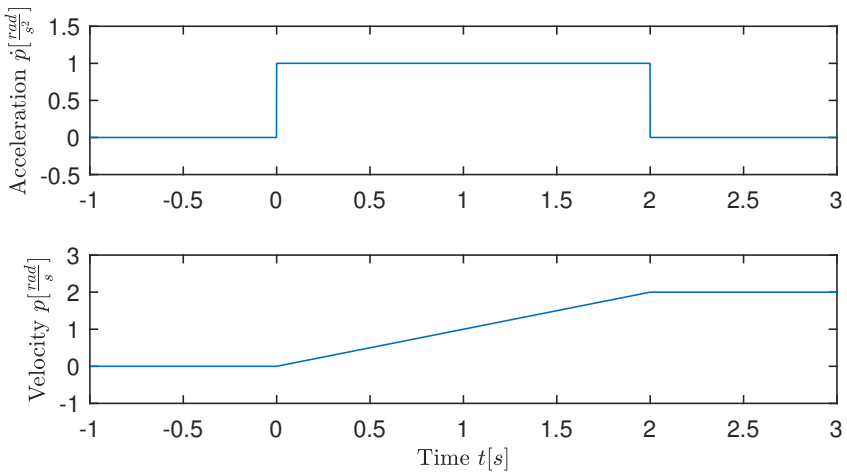

Figure 2.2: Example of scenario with rate change

It is desirable for the change in rate to take a non-infinite amount of time $T[s]$, and for the rate not change before or afterwards, therefore the angular acceleration $\dot{p} = 0$ in other intervals. The value of the integral can be taken as the required change in angular rate Δp $[\frac{rad}{s}]$. If using the simplification of angular acceleration to constant from before, the manoeuvre can be described

as following.

$$\Delta p = \int_0^T \dot{p}\ dt \tag{2.17}$$

$$= \left[\dot{p} \cdot t\right]_0^T \tag{2.18}$$

$$= \dot{p} \cdot T \tag{2.19}$$

$$T = \frac{\Delta p}{\dot{p}} \tag{2.20}$$

The rate change Δp increases with the acceleration applied and length of the impulse, which is here equal to the time of the entire manoeuvre. Last equation shows, that the time required T to execute a change in rate increases with the desired change in rate and decreases with the acceleration applied or available.

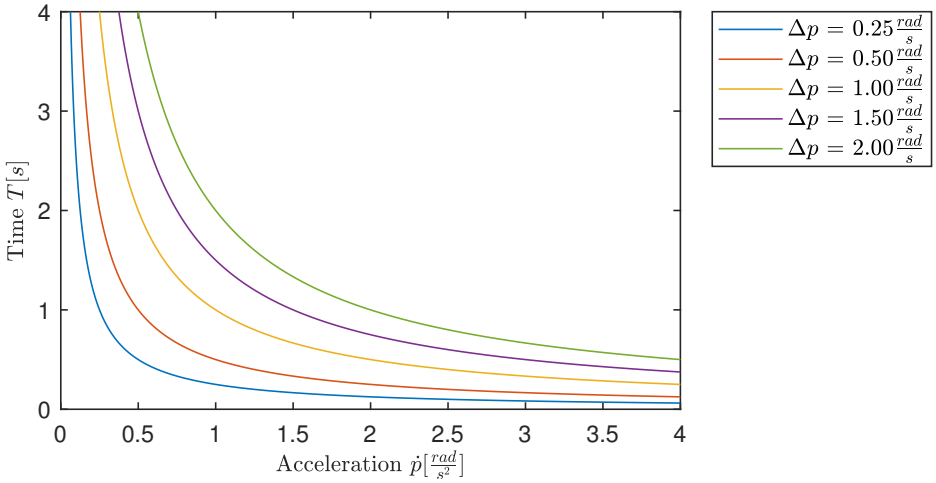

Figure 2.3: Graph of the minimum required time function for rate change

The time-acceleration characteristic has a hyperbolic shape, and it is dependent on the change in rate required. Simply said, the faster the manoeuvre needs to be executed, the more acceleration is required, therefore greater force applied or lesser moment of inertia of the vehicle.

2.2.2 Change in rate with delay

It is common for a system (sensors, control unit, actuators, etc.), not to react instantaneously, therefore adding time delay $\tau[s]$ (which from principle is positive or zero). If all end elements have the same delay, and the simplification

to a constant can be applied, following is the result.

$$\dot{p}(t) = \frac{\sum F_L(t) \times r}{J_x} \tag{2.21}$$

$$= \frac{\sum \left([F_L \cdot i(t-\tau)] \times l\right)}{J_x} \qquad i(t-\tau)\ \epsilon\ [-1, 1] \tag{2.22}$$

$$= \dot{p}(t-\tau) \qquad \dot{p}\ \epsilon\ [\dot{p}_{max}, \dot{p}_{min}] \tag{2.23}$$

It is still the same constant just shifted in time by the delay. Considering that it can be applied to previous equations considering the change in rate Δp.

$$\Delta p(t) = \int_0^T \dot{p}(t-\tau)\ dt \tag{2.24}$$

$$= \int_\tau^T \dot{p}\ dt \tag{2.25}$$

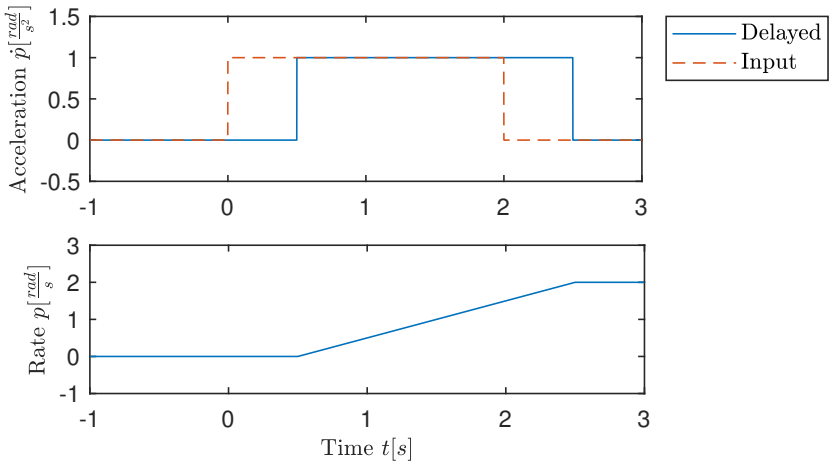

Figure 2.4: Example of scenario with rate change and delay

The result is the same just delayed in time, which is to be expected. Note that the acceleration cannot be performed sooner, as the time delay prevents it. If it did, the signal to begin the manoeuvre would have to start before $t = 0$, which could lead to predictive and/or non-causative behaviour. Further, applying the result to the motion laws as before results in following.

$$\Delta p = \int_\tau^T \dot{p}\ dt \tag{2.26}$$

$$= \left[\dot{p} \cdot t\right]_\tau^T \tag{2.27}$$

$$= \dot{p} \cdot (T - \tau) \tag{2.28}$$

$$T = \frac{\Delta p}{\dot{p}} + \tau \tag{2.29}$$

The result is unsurprising, the change in rate increases with the acceleration applied $\dot{p}$, and the length of the pulse. Therefore, it increases with the overall time of the manoeuvre T, and decreases with the size of the delay τ. Similarly, the time required to execute the change is extended by the time delay τ. Comparing the length of the pulse when the angular acceleration is applied to the vehicle, it remains the same as it is just shifted in time.

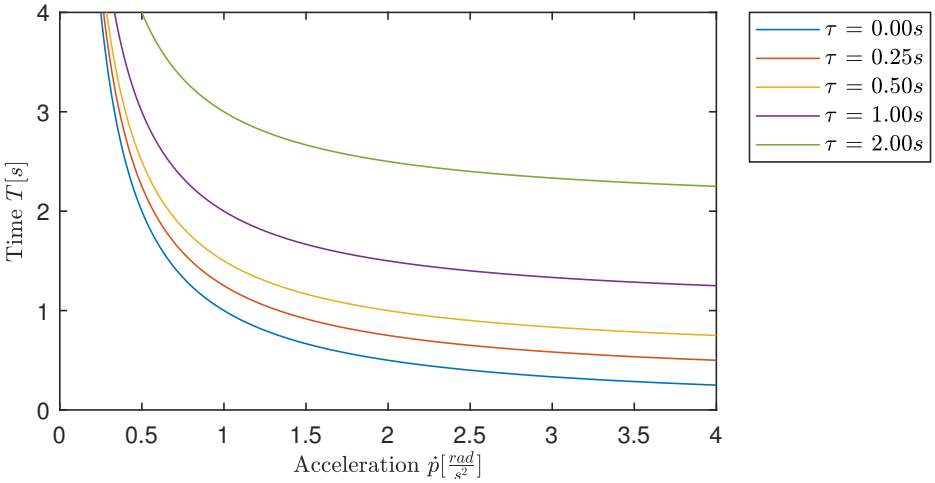

Figure 2.5: Graph of the minimum required time function for rate change with delay

The time-acceleration characteristic has the same shape as before, it only shifts up on the T axis with increasing time delay τ. Therefore, the fastest achievable time T for executing the manouevre is almost equal to the time delay τ, under the condition that the acceleration $\dot{p}$ is almost infinite.

2.2.3 Change in angle

Changing the angle, for example the roll angle, requires changing rate first. It is necessary to accelerate toward the target angle and then decelerate just before it is reached.

For the angle to remain static after the manoeuvre, the final angular rate must be equal to zero. Assuming the initial state is also static, this can be expressed as an integral condition concerning the total change in rate, which is to be equal to zero. In other words, the rate the vehicle accelerated to must be equal to the rate that it decelerated by later.

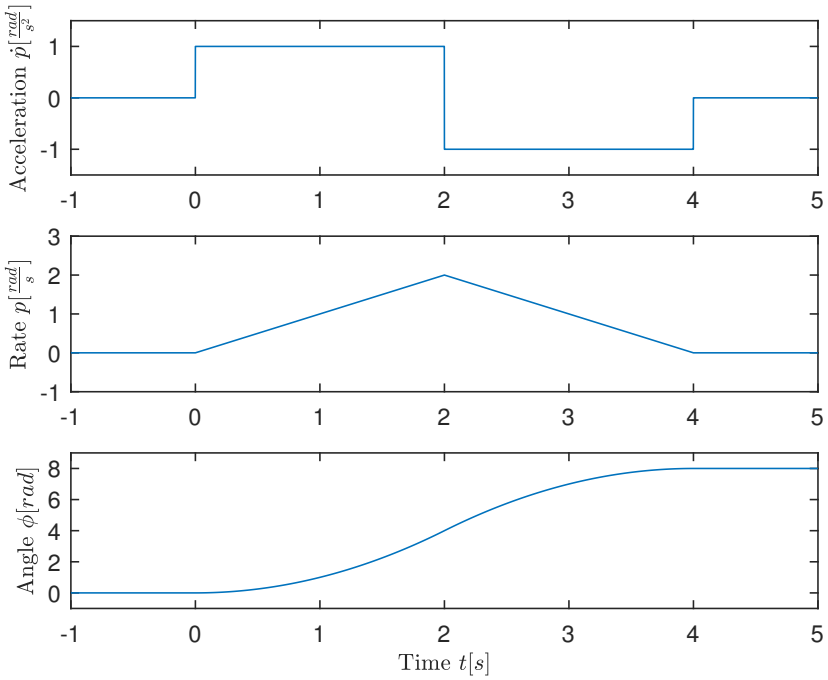

Figure 2.6: Example of scenario with angle change

$$0 = \Delta p \tag{2.30}$$
$$= \int_{-\infty}^{\infty} \dot{p}\ dt \tag{2.31}$$
$$= \int_{-\infty}^{0} 0\ dt + \int_{0}^{T} \dot{p}\ dt + \int_{T}^{\infty} 0\ dt \tag{2.32}$$
$$= \int_{0}^{T} \dot{p}\ dt \tag{2.33}$$

The integral of total acceleration is equal to zero. Splitting it into an acceleration phase and deceleration phase yields following.

$$0 = \int_{0}^{T} \dot{p}\ dt \tag{2.34}$$
$$= \int_{0}^{T_1} \dot{p}_A\ dt + \int_{T_1}^{T} \dot{p}_D\ dt \tag{2.35}$$
$$= \dot{p}_A \cdot T_1 + \dot{p}_D \cdot (T - T_1) \tag{2.36}$$
$$\dot{p}_A \cdot T_A = -\dot{p}_D \cdot T_D \tag{2.37}$$

This formulates a requirement for the time during which acceleration $T_A[s]$ and deceleration $T_D[s]$ take place, relative to angular acceleration and deceleration available. In the case that angular acceleration $\dot{p}_A[\frac{rad}{s^2}]$ is equal to negative

angular deceleration $\dot{p}_D[\frac{rad}{s^2}]$, in other words the acceleration can be applied in both directions the same, it gets simplified accordingly.

$$\dot{p}_A \cdot T_A = -\dot{p}_D \cdot T_D \qquad \dot{p}_D = -\dot{p}_A \tag{2.38}$$

$$T_A = T_D \tag{2.39}$$

The acceleration time T_A is equal to the deceleration time T_D, which are then both equal to half of the total time T required. This is to be expected, as in that scenario it is "symmetrical" in time, rate and acceleration. Now if motion laws for angle are used, they yield the following.

$$\Delta\phi = \int_0^T p(t)\ dt \tag{2.40}$$

$$= \int_0^{T_A} p(t)\ dt + \int_{T_A}^{T} p(t) + p(T_A)\ dt \tag{2.41}$$

$$= \int_0^{T_A} \int \dot{p}_A\ dt\ dt + \int_{T_A}^{T} \Big(\int \dot{p}_D\ dt \Big) + p(T_A)\ dt \tag{2.42}$$

$$= \int_0^{T_A} \int \dot{p}_A\ dt\ dt + \int_{T_A}^{T} \int \dot{p}_D\ dt\ dt + \int_{T_A}^{T} \int_0^{T_A} \dot{p}_A\ dt\ dt \tag{2.43}$$

$$= \Big[\frac{1}{2}\dot{p}_A \cdot t^2\Big]_0^{T_A} + \Big[\frac{1}{2}\dot{p}_D \cdot t^2\Big]_{T_A}^{T} + \Big[\dot{p}_A \cdot T_A \cdot t\Big]_{T_A}^{T} \tag{2.44}$$

$$= \frac{1}{2}\dot{p}_A \cdot T_A^2 + \frac{1}{2}\dot{p}_D \cdot T_D^2 + \dot{p}_A \cdot T_A \cdot T_D \tag{2.45}$$

$$\tag{2.46}$$

There are too many variables to efficiently determine any characteristics from it so far. With the previously formulated requirement, for the relation of time to acceleration, it can be now simplified further.

$$\Delta\phi = \frac{1}{2}\dot{p}_A \cdot T_A^2 + \frac{1}{2}\dot{p}_D \cdot T_D^2 + \dot{p}_A \cdot T_A \cdot T_D \tag{2.47}$$

$$= \frac{1}{2}\dot{p}_A \cdot T_A^2 - \frac{1}{2}\dot{p}_A \cdot T_D \cdot T_A + \dot{p}_A \cdot T_A \cdot T_D \tag{2.48}$$

$$= \frac{1}{2}\dot{p}_A \cdot T_A^2 + \frac{1}{2}\dot{p}_A \cdot T_D \cdot T_A \tag{2.49}$$

$$= \frac{1}{2}\dot{p}_A \cdot T_A(T_A + T_D) \tag{2.50}$$

$$= \frac{1}{2}\dot{p}_A \cdot T_A \cdot T \tag{2.51}$$

To remove time of acceleration T_A from the equation it is necessary to replace it with a function of total time T, angular acceleration $\dot{p}_A$ and deceleration $\dot{p}_D$ together with the requirement formulated before.

$$\frac{T_A}{T} = \frac{T_A}{T_A + T_D} \tag{2.52}$$

$$= \frac{T_A}{T_A - \frac{\dot{p}_A}{\dot{p}_D} T_A} \tag{2.53}$$

$$= \frac{1}{1 - \frac{\dot{p}_A}{\dot{p}_D}} \tag{2.54}$$

If substituted into the equation, following result will emerge.

$$\Delta\phi = \frac{1}{2}\dot{p}_A \cdot T^2 \frac{T_A}{T} \tag{2.55}$$

$$= \frac{1}{2}\dot{p}_A \cdot T^2 \frac{1}{1 - \frac{\dot{p}_A}{\dot{p}_D}} \tag{2.56}$$

$$= \frac{T^2}{2} \cdot \frac{\dot{p}_A}{1 - \frac{\dot{p}_A}{\dot{p}_D}} \tag{2.57}$$

$$T = \sqrt{2 \cdot \Delta\phi \cdot \frac{1 - \frac{\dot{p}_A}{\dot{p}_D}}{\dot{p}_A}} \tag{2.58}$$

The resulting equations show that the angle change increases with the square of the time required T. The time required to execute a specified change in angle decreases with angular acceleration and deceleration available and is further affected by the ratio of angular acceleration and deceleration. The equation further simplifies in the previously mentioned case in which angular acceleration $\dot{p}_A$ is equal to negative angular deceleration $\dot{p}_D$.

$$\Delta\phi = \frac{T^2 \cdot \dot{p}}{4} \tag{2.59}$$

$$T = 2\sqrt{\frac{\Delta\phi}{\dot{p}}} \tag{2.60}$$

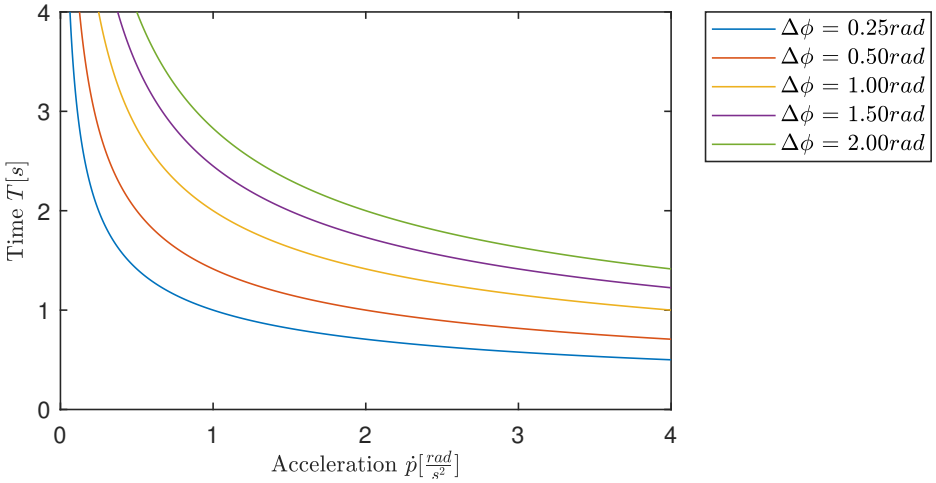

Figure 2.7: Graph of the minimum required time function for angle change with the condition $\dot{p}_A = -\dot{p}_D$

The time-acceleration graph has the shape of a skewed hyperbola, which is caused by the square root in the function. It is comparatively more demanding to reach a shorter time T, but that is to be expected, since the rate needs to change twice.

To get some perspective on the ratio of acceleration to deceleration, the result needs to be rearranged. If it is rearranged that, so it expresses either acceleration or deceleration, then it should be possible to determine what effect the ratio has on the time required.

$$\Delta\phi = \frac{T^2}{2} \cdot \frac{\dot{p}_A}{1 - \frac{\dot{p}_A}{\dot{p}_D}} \tag{2.61}$$

$$\frac{2\Delta\phi}{T^2 \cdot \dot{p}_A} = \frac{1}{1 - \frac{\dot{p}_A}{\dot{p}_D}} \tag{2.62}$$

$$1 - \frac{T^2 \cdot \dot{p}_A}{2\Delta\phi} = \frac{\dot{p}_A}{\dot{p}_D} \tag{2.63}$$

$$\frac{1}{\dot{p}_A} - \frac{T^2}{2\Delta\phi} = \frac{1}{\dot{p}_D} \tag{2.64}$$

$$\dot{p}_D = \frac{1}{\frac{1}{\dot{p}_A} - \frac{T^2}{2\Delta\phi}} \tag{2.65}$$

This result isn't easily interpretable as is, but can be graphed.

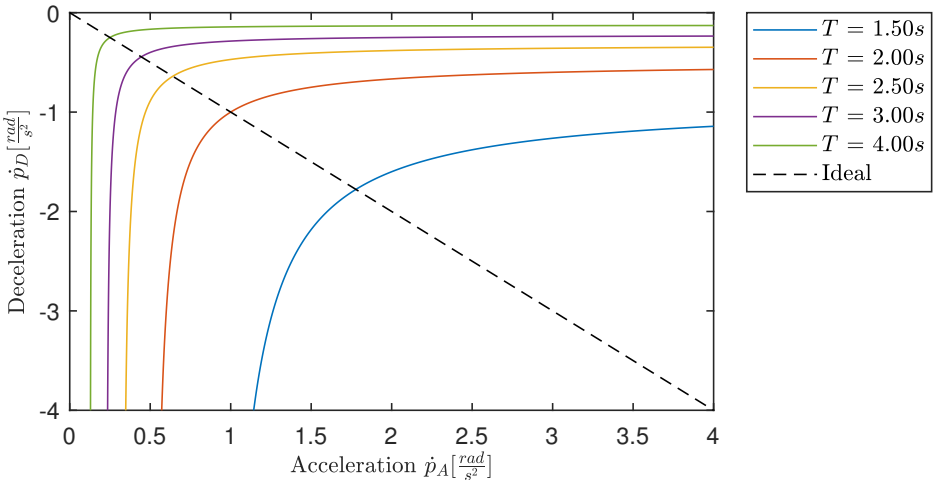

Figure 2.8: Graph of the minimum required time function for angle change with regard to the ratio of the acceleration to deceleration

The graph of acceleration to deceleration has also a hyperbolic shape. The isochronic lines show that the most efficient ratio is 1:-1 (highlighted by the dashed line), as it is closest to the point $\dot{p}_A = 0, \dot{p}_D = 0$ on every line. That means it is less efficient to increase only acceleration or deceleration, to shorten the time that the target angle is reached, then increasing both equally. This ideal ratio is then also indifferent to the direction of the change in angle, as it can be inverted without change.

The total time could be further affected by delay τ. It would have a similar

effect as before. The translation between acceleration and deceleration does not have to be affected by it, because the sequence can be precalculated and predictively performed.

2.3 Reaction to disturbance

2.3.1 Constant disturbance

The simplest example of this is gravity, which is a force that must be overcome by any successful flying vehicle. It causes acceleration of approximately $g = 9.8\frac{m}{s^2}$ near the Earth's surface. If the vehicle is level with the horizon $i.e. \phi, \theta = 0$, the acceleration applies in the Z-direction.

$$\dot{w}(t) = g - \dot{w}(t) \tag{2.66}$$

$$= \dot{w} \qquad \dot{w} \; \epsilon \; [g - \dot{w}_{max}, g - \dot{w}_{min}] \tag{2.67}$$

The total acceleration is a sum of the acceleration caused by propulsion of the vehicle $\dot{z}[\frac{m}{s^2}]$ and the acceleration caused by gravity. Therefore, the vehicle does not accelerate when $\dot{w} = g$.
This does not affect the vehicle much in terms of delay-sensitive control, as the disturbance is not changing. It only moves the window of available acceleration, or in other terms it changes values that can total acceleration $\dot{w}$ be.

2.3.2 Effect on rate

An example of this are wind gusts. Assuming the wind gust can cause a translational or rotational error, they can be modelled as their simplest form with a step function.

$$\dot{p}_E(t) = \frac{\sum L_E(t)}{J_x} \tag{2.68}$$

$$= \dot{p}_E \qquad t \geq 0 \tag{2.69}$$

$$= 0 \qquad t < 0 \tag{2.70}$$

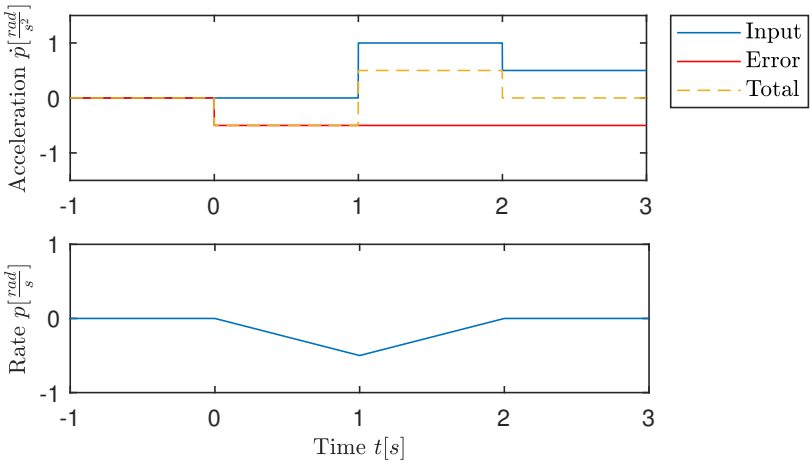

Figure 2.9: Example of scenario with rate affected by a step disturbance

The acceleration caused by the error $\dot{p}_E(t)[\frac{rad}{s^2}]$ must be counteracted by the acceleration caused by the propulsion $\dot{p}_T(t)[\frac{rad}{s^2}]$ An acceleration equilibrium is reached when $\dot{p}_E = -\dot{p}_T$, which is the desired end state. When this state is not reachable (i.e. $|\dot{p}_T| - |\dot{p}_E| < 0$ & $sign(\dot{p}_T) = sign(\dot{p}_E)$), the error acting on the vehicle cannot be counteracted.

If no time delay τ was present in the propulsion system, and the end state is reachable, the acting error could be mitigated instantly. But that is a practically impossible scenario, as some time is required to obtain (or measure) the amplitude of the error step function $\dot{p}_E$. Since the system now has a delay, the error acceleration creates an error in rate Δp_E, before the propulsion can react.

$$\Delta p_E = \int_0^\tau \dot{p}_E \, dt \tag{2.71}$$

$$= \dot{p}_E \cdot \tau \tag{2.72}$$

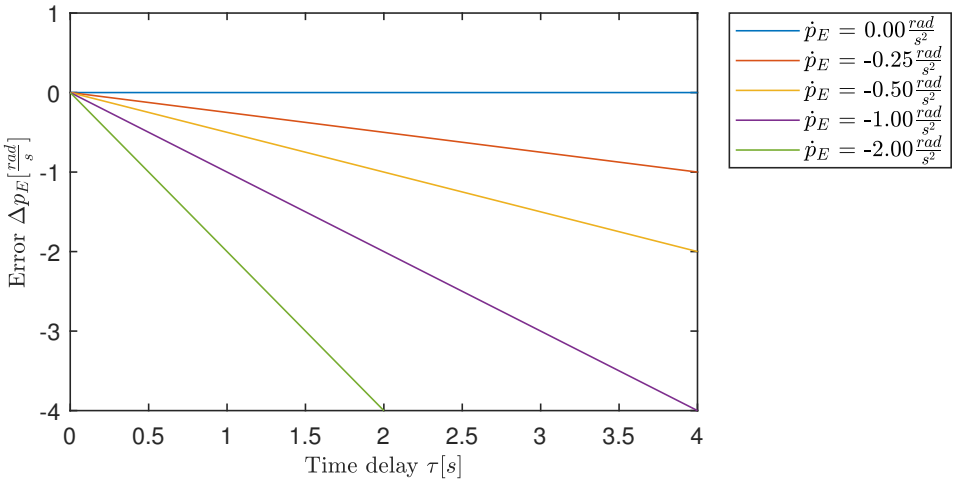

Figure 2.10: Graph of the rate error function

The result shows that the error in rate $\Delta p_E[\frac{rad}{s}]$ increases linearly with the amplitude of the error $\dot{p}_E$ and the time delay τ. To return the rate to the original value, the vehicle must change its rate by $-\Delta p_E$. Using the previously gained equation for the change in rate with delay (during which the error in rate was forming) and the substitution of $\dot{p} = \dot{p}_T + \dot{p}_E$, following is the result.

$$T = \frac{-\Delta p_E}{\dot{p}_T + \dot{p}_E} + \tau \tag{2.73}$$

$$= \frac{-\dot{p}_E \cdot \tau}{\dot{p}_T + \dot{p}_E} + \tau \tag{2.74}$$

$$= \frac{\dot{p}_T \cdot \tau}{\dot{p}_T + \dot{p}_E} \tag{2.75}$$

The time to counteract the error T increases with the delay τ in the system and with the acceleration ratio of the error to the propulsion $\frac{\dot{p}_E}{\dot{p}_T}$.

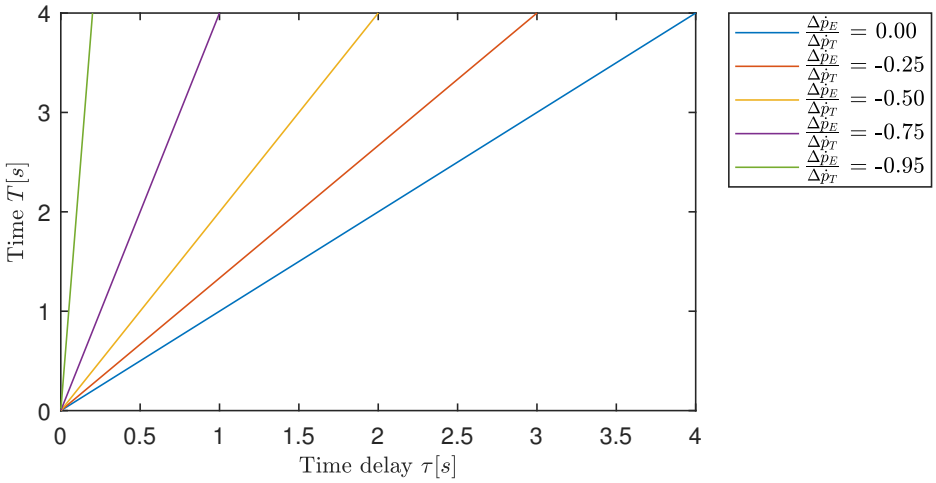

(a) : As a function of time delay

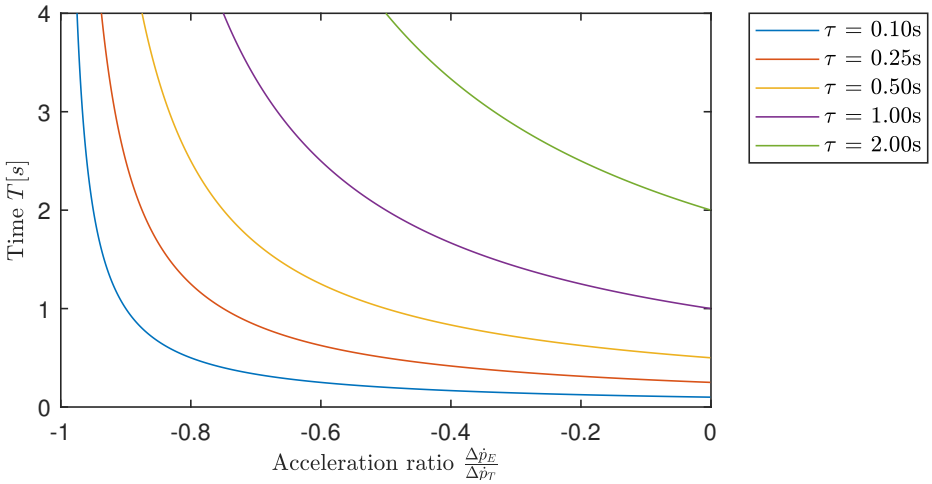

(b) : As a function of disturbance to propulsion ratio

Figure 2.11: Graphs of settling time function for rate error

Both the error in rate Δp and the settling time T increase only linearly with the time delay τ. The acceleration $\dot{p}_E$ changes the steepness of the characteristic, with the acceleration caused by the propulsion $\dot{p}_T$ having an inverse effect. The settling time is of course limited by the time delay τ as its minimum value.

2.3.3 Effect on angle

An extension of previous example, where angle is also considered for correction too. During the counteracting of the rate, which will take time T_1 expressed

before, the angle will be changed by $\Delta\phi_E[rad]$.

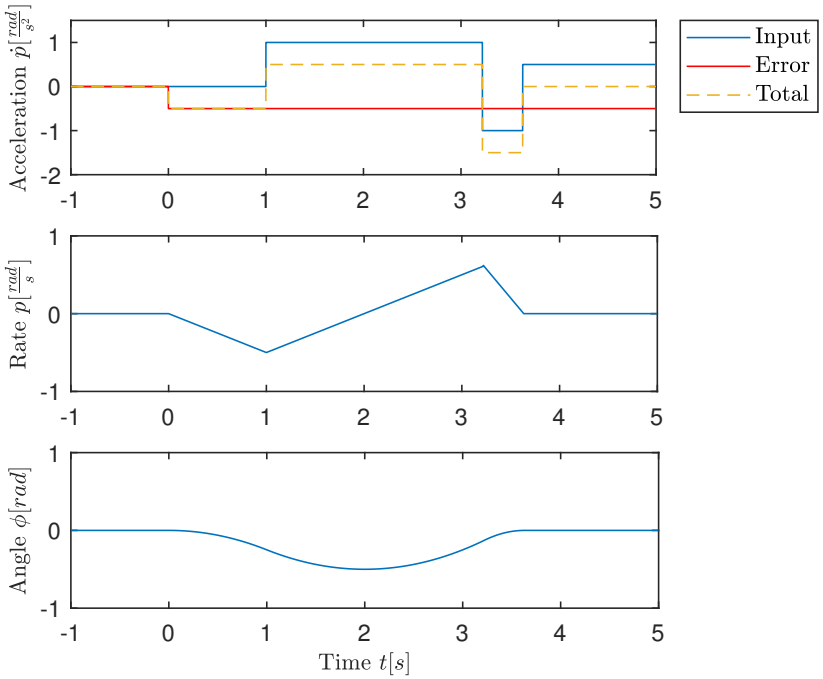

Figure 2.12: Example of scenario with angle and rate affected by a step disturbance

We can substitute the acceleration $\dot{p}_A = \dot{p}_E$ and deceleration $\dot{p}_D = \dot{p}_E + \dot{p}_T$ in the equation for change in angle to avoid repeated integration.

$$\Delta\phi_E = \frac{T_1^2}{2} \cdot \frac{\dot{p}_E}{1 - \frac{\dot{p}_E}{\dot{p}_E + \dot{p}_T}} \tag{2.76}$$

$$= \frac{(\frac{\dot{p}_T \cdot \tau}{\dot{p}_T + \dot{p}_E})^2}{2} \cdot \frac{\dot{p}_E}{\frac{\dot{p}_T}{\dot{p}_E + \dot{p}_T}} \tag{2.77}$$

$$= \frac{\tau^2}{2} \cdot \frac{\dot{p}_T \cdot \dot{p}_E}{\dot{p}_T + \dot{p}_E} \tag{2.78}$$

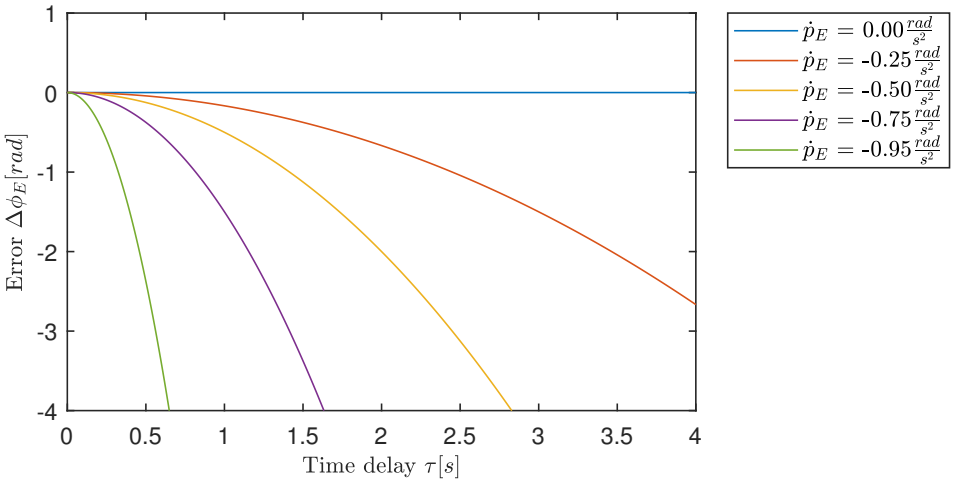

Figure 2.13: Graph of the angular error function

The error in angle increases with the square of the time delay τ, unlike before with rate, due to it being the second integral. Now it is possible to calculate the time T_2, that will be needed to return to the original angle, substituting $\Delta\phi = -\Delta\phi_E$, $\dot{p}_A = \dot{p}_E + \dot{p}_T$ and $\dot{p}_D = \dot{p}_E - \dot{p}_T$ in the equation for the change in angle.

$$T_2 = \sqrt{2 \cdot -\Delta\phi_E \cdot \frac{1 - \frac{\dot{p}_E + \dot{p}_T}{\dot{p}_E - \dot{p}_T}}{\dot{p}_E + \dot{p}_T}} \tag{2.79}$$

$$= \sqrt{2 \cdot -\frac{\tau^2}{2} \cdot \frac{\dot{p}_T \cdot \dot{p}_E}{\dot{p}_T + \dot{p}_E} \cdot \frac{\frac{-2\dot{p}_T}{\dot{p}_E - \dot{p}_T}}{\dot{p}_E + \dot{p}_T}} \tag{2.80}$$

$$= \tau \cdot \frac{\dot{p}_T}{\dot{p}_T + \dot{p}_E} \sqrt{\frac{2 \cdot \dot{p}_E}{\dot{p}_E - \dot{p}_T}} \tag{2.81}$$

This result shows, that the time is still linearly dependent on the time delay τ. To get the total time T that is required to get to the original angle, from the start of the error's effect, the result needs to be added up with T_1.

$$T = \tau \cdot \frac{\dot{p}_T}{\dot{p}_T + \dot{p}_E} \sqrt{\frac{2 \cdot \dot{p}_E}{\dot{p}_E - \dot{p}_T}} + \frac{\dot{p}_T \cdot \tau}{\dot{p}_T + \dot{p}_E} \tag{2.82}$$

$$= \tau \cdot \frac{\dot{p}_T}{\dot{p}_T + \dot{p}_E} \left(\sqrt{\frac{2 \cdot \dot{p}_E}{\dot{p}_E - \dot{p}_T}} + 1 \right) \tag{2.83}$$

The required time T increases linearly with the time delay τ and the acceleration caused by the external factor $\dot{p}_E$. Inversely, it decreases with the acceleration of the propulsion $\dot{p}_T$. This result can be also seen as an extension of the previous result for rate as the only difference is the square root in the brackets.

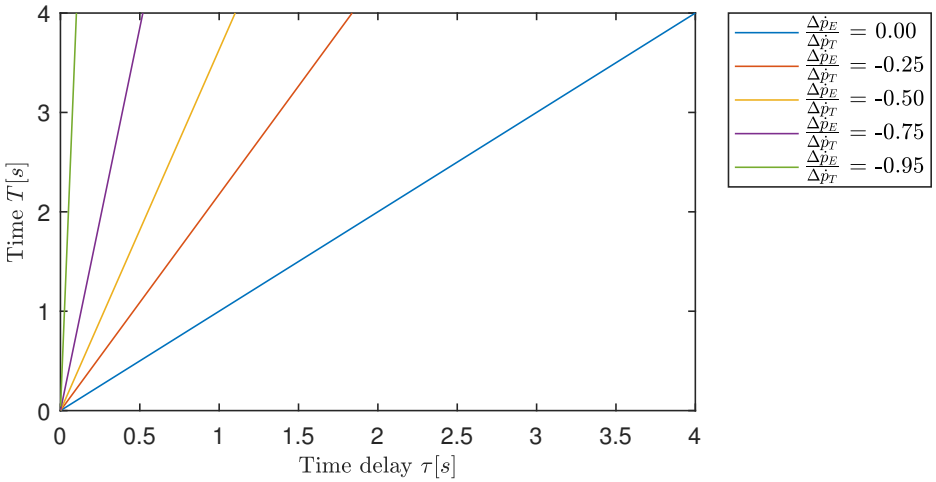

(a) : As a function of time delay

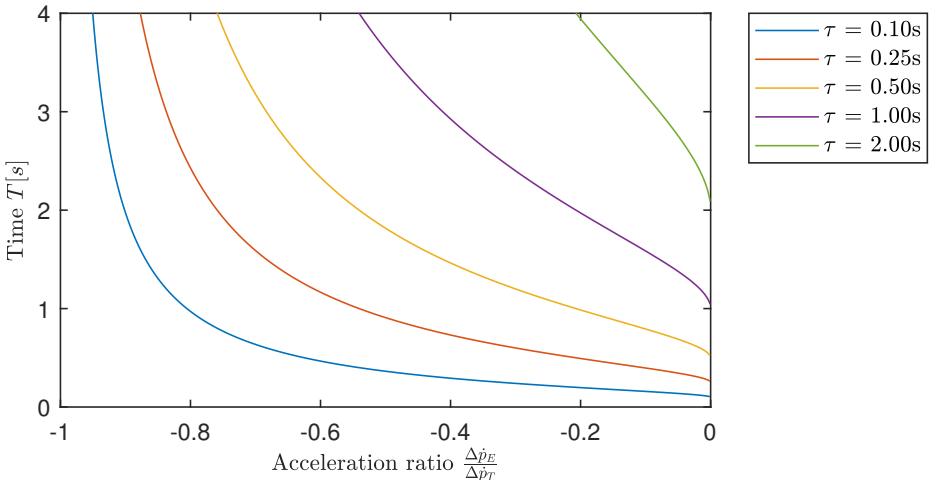

(b) : As a function of disturbance to propulsion ratio

Figure 2.14: Graphs of settling time function for angular error

The error in angle $\Delta\phi$ follows a parabola in relation to the time delay τ. On the contrary, the settling time T still gets reduced to a linear function in relation to the time delay τ. The graph for the settling time T in relation to the acceleration ratio $\frac{\dot{p}_E}{\dot{p}_T}$ shows that the time required increases rapidly with any time delay τ, even for small values of the ratio.

Chapter 3

eVTOL modelling

To obtain more realistic data a simulation model is necessary. First, a model of the hypothetical civilian eVTOL is required to obtain aerodynamic characteristics to use in the simulation. Then, Simulink and MATLAB will be used to create a simulation model from the derived subsystems. Standard assumed conditions are the speed of sound $c = 343\ \frac{m}{s}$ and air density $\rho = 1.2\ \frac{kg}{m^3}$.

3.1 Aerodynamic model

For the aerodynamic model creation freely available OpenVSP software was used, which provides an environment for modelling aeroplanes and aerodynamics related applications. To analyse aerodynamic characteristics the integrated VSPAero tool is used, which provides static analysis of the modelled structure. The modelling workflow consists of parametrizing properties of different parts, such as wings, fuselages and propellers, and defining their position in the workspace or relative to each other.

The inspiration for the eVTOL section if of this model was the Zuri 2.0, but there are certain alterations. Overall, the modelled aeroplane is a six engined eVTOL aeroplane with a high-wing and a V-tail. Compared to Zuri it lacks two engines on the V-tail, otherwise the VTOL configuration is similar.

The fuselage is 15 m in length, roughly teardrop shaped length-wise. Its cross-section is a 2x2 m rounded square cross-section in the main section. Nose of the fuselage is lowered down, and the tail section is raised up.

The main wing is blended to the top of the fuselage, it has a wingspan of $b = 16$ m and a 0° sweep on the leading edge. Chord of the main wing increases closer to the fuselage, the overall shape of the main wing's trailing edge improves the behaviour of the trailing wakes separating from the wing, more so with higher angle of attack. There are 2 pods for mounting engines on each main wing, one at the distance of 3.5 m from the fuselage and other at the end of the wing. The propellers are $d = 3.5m$ in diameter, each is mounted at a distance of 1.75 m in the front of the main wing, so the airflow does not get obstructed by the wing, which would hinder performance. For quick reconfiguration a hinge is included between the propeller and the engine pod, but the hinge has no aerodynamic model on its own.

The surfaces of the V-tail are 5 m in span and at a 135° angle. They have a 20° sweep and decrease in chord from 2.5 m to 1.5 m away from the fuselage. At the end of the wing an engine mounting pod is located with the same propeller at the front. Originally an attempt on using a more conventional tail was made, but the airflow behind the main wing severely affected the lift produced by the elevator, possibly rendering the aircraft unstable near low angles of attack.

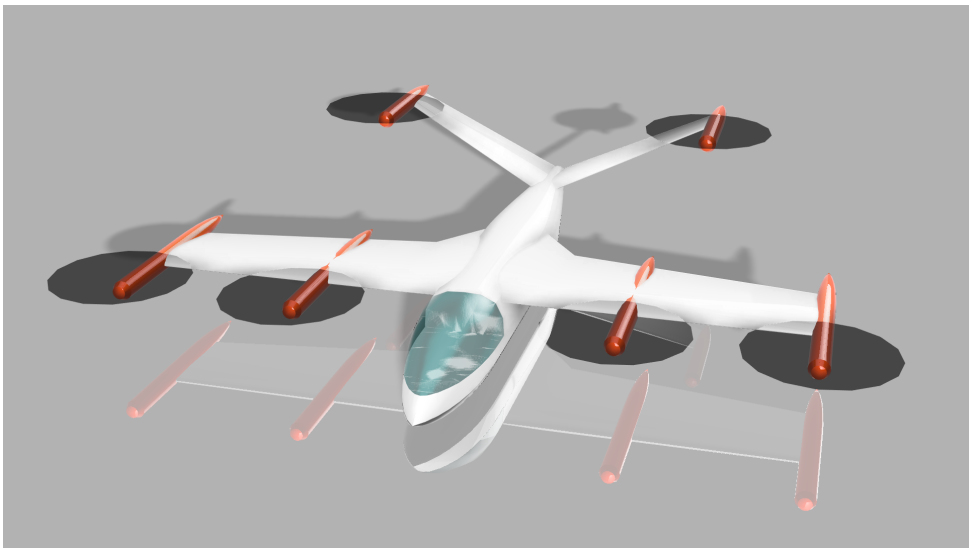

Figure 3.1: Render of the modelled eVTOL aircraft

Since this is a theoretical model, a similar sized light aircraft can be selected as a starting point for weight and inertia estimates. The Cessna 172 [Cel19]

is a four-seat aircraft, that is fairly well documented. Compared to it, the modelled aircraft has 1.36x larger wingspan and is 1.81x longer. From that a rounded estimate on inertia of $J_x = 3500\ kg \cdot m^2$ can be reached, using a factor of 1.44. The same can be done with maximum takeoff weight to get an estimate of $m_0 = 2000\ kg$, with a factor of 1.73.

3.1.1 Propeller characteristics

To correctly model the propellers in VSPAero their coefficients of thrust and power are required, together with the current revolutions per minute $n[RPM]$. The coefficient of thrust and power graph is dependent on the blade angle $\theta_{3/4}[°]$ at $\frac{3}{4}$ of the propeller's radius and advance ratio [McC79], which is a function of airspeed $u_0[\frac{m}{s}]$, the diameter of the propeller $D[m]$ and revolutions per second, which can be converted to revolutions per minute n.

$$J = \frac{60u_0}{Dn} \tag{3.1}$$

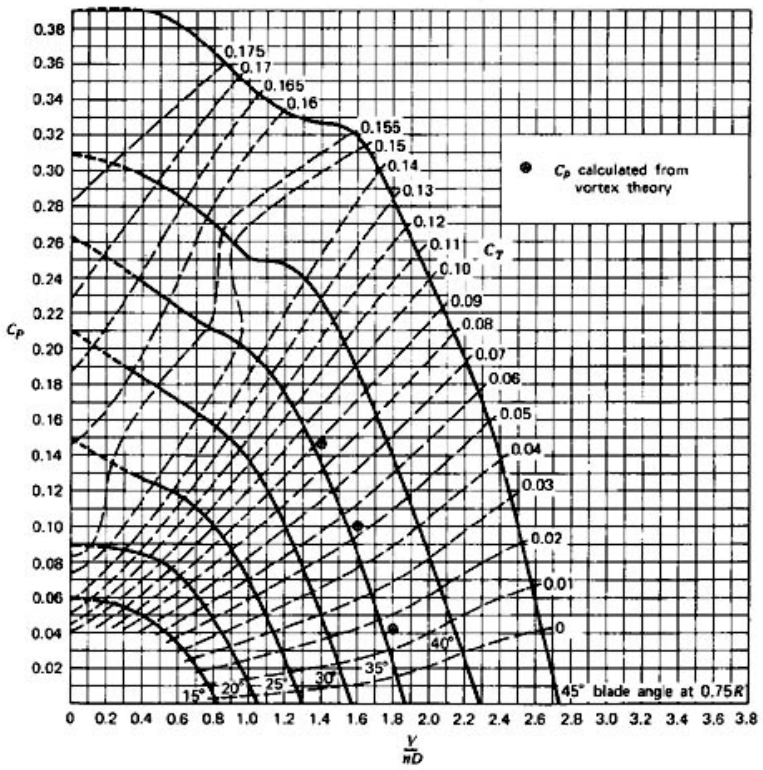

Figure 3.2: Coefficient of thrust and power graph [McC79]

For hover the value of the advance ratio J can be assumed 0, because the vertical airspeed close to zero, for forward flight with this modelled aeroplane, airspeed of Mach 0.3 and $n_0 = 900\ RPM$ the advance ratio J is 1.96. The typical propeller thrust curves give the coefficient of thrust $C_T[-]$ for hover around 0.16 with the blade angle $\theta_{3/4}$ of 20° and for forward flight around 0.10 with the blade angle $\theta_{3/4}$ of 45°. That also allows to calculate the propeller's thrust [Joh13], which can reversely be used to estimate the required n_0 necessary for hover.

$$T = \frac{1}{2}\rho(\omega R)^2(\pi R^2)C_T \tag{3.2}$$

$$\omega = 2\pi\frac{n}{60} \tag{3.3}$$

$$v_{tip} = \omega R \tag{3.4}$$

The required total thrust $T_6[N]$ for hover with the maximum takeoff weight is approximately 20 kN, which using the previous values gives the n_0 of 327.815 RPM.

VSPAero also requires the propeller tip speed when in hover. The propeller tip speed $v_{tip}[\frac{m}{s}]$ should stay under Mach 1 [Joh13], which would occur around $n_0 = 1500\ RPM$. Otherwise, it could have adverse effects, including decreased thrust efficiency.

Unfortunately the VTOL configuration does not converge to its solution with the reference speed set to zero. For hover a low forward speed u_0 of 10 $\frac{m}{s}$ will be assumed, which would however be insufficient for regular flight.

Parameter	Symbol	Hover	Forward flight
Flight speed	u_0	$10\frac{m}{s}$	$102.9\frac{m}{s}$
Thrust coefficient	C_T	0.16	0.10
Power coefficient	C_P	0.09	0.24
Angle of the blade	$\theta_{3/4}$	20°	45°
Propeller rotational speed	n	327.815 RPM	900 RPM
Propeller tip speed	v_{tip}	$60.075\frac{m}{s}$	$164.934\frac{m}{s}$
Propeller thrust	T	3333.3 N	15703 N
Combined propeller thrust	T_6	20 000 N	94221 N

Table 3.1: Flight conditions and propeller characteristics for the modelled aircraft

There is also a rotating blade mode for simulating propellers in VSPAero, but there is insufficient information to model the entire blades, as chord, twist and thickness of the blades.

3.1.2 Flight stability analysis

The model was created with certain flight stability requirements on all the moment axis with regard to angle of attack $\alpha[°]$.

Firstly, the roll and yaw moments should be near zero, in other words no rolling or yawing moment should be caused by pitching up. The other requirement is for the pitch moment, as it should counter the angle of attack, therefore acting as a stable feedback loop. Therefore, the value of the pitching moment should be negatively proportional to the angle of attack. Usually it also contains a small negative bias, which should be countered with trimming of the elevator.

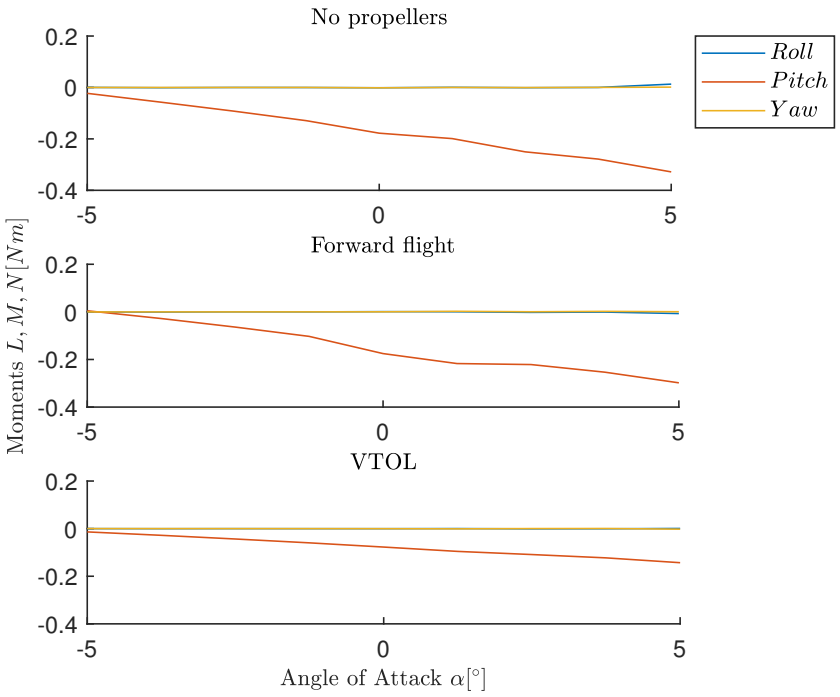

Figure 3.3: Moments about all axis as functions of angle of attack

The moment analysis seems satisfactory, as conditions specified were met.

3.1.3 Stability coefficients and derivatives

Dimensionless stability coefficients and derivatives are an important metric for creating simulation models and comparing different aircraft. To obtain the derivatives VSPAero in the static stability mode is used.

The coefficients are used to calculate forces, such as lift, drag and crosswind force, and moments about the roll, pitch and yaw axis [Ste15]. They are dependent on a wide array of conditions, such as velocities, control surface deflections and angles relative to wind. To analyse them further the coefficients are defined as a sum of derivatives with regard to these changing conditions.

$$
\begin{aligned}
X &= QSC_D \\
Y &= QSC_C \\
Z &= QSC_L \\
L &= QSbC_l \\
M &= QScC_m \\
N &= QSbC_n
\end{aligned}
$$

Table 3.2: Equations for aerodynamic forces and moments containing dimensionless stability coefficients

Dynamic pressure $Q[\frac{kg}{m \cdot s^2}]$ is common in all the equations, it is a function of air density and airspeed [Cau11]. When airspeed is zero, the dynamic pressure Q is also zero, therefore aerodynamic moments don't apply.

$$
Q = \frac{1}{2}\rho u_0^2 \tag{3.5}
$$

$$
\begin{aligned}
C_D &= C_D^0 + \Delta C_D^{\delta e} + \Delta C_D^{\delta r} + \Delta C_D^{\delta a} + \Delta C_D^{\delta f} + \dots \\
C_L &= C_L^0 + \Delta C_L^{\delta e} + \Delta C_L^{\delta f} + \dots \\
C_C &= C_C^0 + \Delta C_C^{\delta r} + \Delta C_C^{\delta a} + \tfrac{b}{2u_0}(C_C^p p + C_C^r r) + \dots \\
C_l &= C_l^0 + \Delta C_l^{\delta a} + \Delta C_l^{\delta r} + \tfrac{b}{2u_0}(C_l^p p + C_l^r r) + \dots \\
C_m &= C_m^0 + \Delta C_m^{\delta e} + \tfrac{c}{2u_0}(C_m^q q + C_m^{\dot{\alpha}}) + \tfrac{x_r}{c} C_L + \delta C_m^T + \dots \\
C_n &= C_n^0 + \Delta C_n^{\delta r} + \Delta C_n^{\delta a} + \tfrac{b}{2u_0}(C_n^p p + C_n^r r) + \dots
\end{aligned}
$$

Table 3.3: Definitions of dimensionless stability coefficients as sums of stability derivatives

Many of these coefficients have a similar form in regard to their derivative representation, most noticeably roll and yaw coefficients. They are both

affected by the ailerons and the rudder and have dampening coefficients due to rolling and yawing motion.

The derivatives with the Δ can be ignored for now, as no surface controls have been modelled.

Some derivatives are almost universally equal to zero, such as rolling coefficient in regard to elevator deflection. Therefore, they aren't usually mentioned in the definitions at all.

Also note the usage with the last four dampening coefficients and their dampening derivatives. This form also ensures unit cohesion.

Results

To get the derivative values the analysis has been run on the model in different configurations. First, to get the baseline, the model was analysed without any propellers attached in both flight scenarios, to examine the basic behaviour. Later, the propellers have been set to both configurations, to examine the in-flight values for forward flight and VTOL configuration. To make sure the values are within the realm of possibly they can be compared with some real aircraft.

Final VSPAero settings for simulation were 200 iterations for each to ensure convergence, and 128 wake nodes. Overall, the configurations without propellers converged almost always, the forward configuration converged in most cases, however the VTOL configuration did converge poorly at certain reference velocities.

Due to the Vortex Lattice Method (VLM), the drag coefficient result was fairly inconclusive, as the fuselage doesn't get sufficiently taken into account, therefore it can't be compared with other aircraft. For drag simulations, and some other applications the Panel Method is more suitable, although more computationally expensive.

Aircraft	$C_L^0[-]$	$C_l^p[-]$	$C_l^\beta[-]$	$C_n^r[-]$
Model (FF, NP)	0.236	-0.509	-0.193	-0.141
Model (FF)	0.193	-0.514	-0.020	-0.124
Model (VTOL, NP)	0.230	-0.531	-0.020	-0.094
Model (VTOL)	0.116	-0.209	-0.086	-0.043
Cessna 172 [LL57]	0.310	-0.470	-0.089	-0.099
Boeing 747 [RKH72]	1.110	-0.450	-0.221	-0.300
F-4 Phantom II [RKH72]	0.915	-0.272	-0.156	-0.320

Table 3.4: Comparison of dimensionless stability derivatives for different configurations of the model and other aircraft

The coefficient of lift $C_L^0[-]$ is comparatively lower with the modelled eVTOL, as the fuselage may not be accounted for properly with the VLM. The roll dampening derivative $C_l^p[-]$ of the model is in the ranges of civilian aircraft, although it is lower in the VTOL configuration, likely due to wakes from the propellers. On a fighter aircraft like the F-4, the derivative is lower to accommodate higher manoeuvrability at the cost of stability and handling. The sideslip-roll derivative $C_l^\beta[-]$ is higher with aircraft that have dihedrals on wings. The yaw dampening derivative $C_n^r[-]$ of the model is also comparatively similar to the Cessna 172.

The stability analysis also provides the aerodynamics neutral point on the X axis, in this case the distance is from the nose of the aircraft. This is useful for balancing the aircraft with regard to centre of mass.

Configuration	Neutral point position $[m]$
Forward Flight, No Propellers	7.58
Forward Flight	6.99
VTOL, No Propellers	7.42
VTOL	6.27

Table 3.5: Aerodynamic neutral point on the X-axis for different configurations of the model

Without propulsion the neutral point is around 7.5 m. With propulsion the neutral point moves forward, due to the influence of the propellers on the main wing. This change would cause the aeroplane to pitch up. On the other hand, the placement of the propellers would cause for the aircraft to pitch down.

3.2 Roll axis model

A Simulink model of the roll axis can be created from the gathered data.

Main wing area	S	52.5 m^2
Main wing span	b	16 m
Propeller diameter	d	3.5 m
Propeller thrust coefficient	C_T	0.16
Hover RPM	n_0	378.525 RPM
Inertia on the X axis	J_x	3500 $kg \cdot m^2$
Roll dampening derivative	C_l^p	-0.209
Sideslip-roll derivative	C_l^β	-0.086

Table 3.6: Overall characteristics for the roll axis of the modelled aircraft

3.2.1 Aerodynamic dampening model

Since the aerodynamic coefficients and their respective dampening coefficients create a relation between the rate and moment, it is possible to close the loop [Pra00]. Moment has a relation to angular acceleration through inertia, and rate is an integral of angular acceleration.

$$L_p = QSbC_l = QSb\frac{b}{2u_0}C_l^p p \tag{3.6}$$

$$C_p = \frac{1}{J_x}\frac{\partial L_p}{\partial p} = \frac{QSb^2}{2J_x u_0}C_l^p \tag{3.7}$$

This can be simplified to a 1st order system through following simplification.

$$G = \frac{\frac{1}{s}}{1 - \frac{C_p}{s}} = \frac{1}{s - C_p} \tag{3.8}$$

Note that the C_p is always negative under regular conditions, therefore the pole in the system is stable.

3.2.2 Wind gust model

Similar equation as before can be used, but with a different derivative. Assuming the wind gust comes from the side, the sideslip derivative is suitable

[Cau11].

$$L_v = QSbC_l = QSbC_l^\beta \beta = QSbC_l^\beta tan^{-1}(\frac{v}{u_0}) \approx QSbC_l^\beta \frac{v}{u_0} \tag{3.9}$$

$$C_v = \frac{1}{J_x}\frac{\partial L_v}{\partial v} = \frac{QSb}{J_x u_0} C_l^\beta \tag{3.10}$$

This can be implemented as a gain from the wind velocity to angular acceleration.

For model of the wind, 1-cos model can be used [Lea08]. It takes following form, where $v_m[\frac{m}{s}]$ is the maximum magnitude, and $d_m[m]$ is half the length of the gust.

$$v = \frac{v_m}{2}(1 - cos(\frac{\pi x}{d_m})) \tag{3.11}$$

The distance $x[m]$ reaches values from 0 to 2 d_m in one gust, in simulation it is a linear function of time. Three wind scenarios should be sufficient. First is a long stronger gust that should simulate an open area. The second is a shorter but weaker gust that might occur in a more obstructed area when wind changes direction. Lastly, a step function to compare to the analytical formulations from previous chapter.

Scenario	Function shape	Speed $v_m[\frac{m}{s}]$	Length $d_m[m]$
1	1-cos	10	400
2	1-cos	5	50
3	Step	10	-

Table 3.7: Wind scenarios

3.2.3 Propulsion models

To roll the eVTOL in a controlled manner some sort of propulsion is necessary. The obvious first choice is to use the main propellers, specifically the ones on the ends of main wings. The other option is to add an alternative form of propulsion such as a cold gas thruster, which could work similarly to reaction control systems on previously mentioned VTOL aircraft.

Any propulsion method will be affected by delay of the control systems and actuators. For this case $\tau_0 = 100\ ms$ will be sufficient as an example of system delay [DMH12].

$$G_d = e^{-\tau_0 s} \tag{3.12}$$

Thruster

The most pressing concern with the cold gas thruster is the amount of thrust it can generate, which causes a saturation in the control loop. It can be assumed that it reacts much faster than the propellers. Two thrusters at the end of the wings, producing thrust in opposite directions to create the rolling motion will create acceleration equal to following.

$$\dot{p}_t = \frac{b}{I_x} T * i(t) \qquad i(t) \; \epsilon \; [-1, 1] \tag{3.13}$$

$$G_T = \frac{\frac{b}{I_x} T}{\tau s + 1} \tag{3.14}$$

The typical ramp-up time τ in such a propulsion system is around hundreds of milliseconds, and the thrust is in the higher hundreds of Newtons [DMH12]. For the simulation a thrust $T = 1000\ N$ and ramp-up times between 200 ms and 500 ms were selected. That gives a maximum acceleration $\dot{p}_t$ of 4.57 $\frac{m}{s^2}$.

Main propeller

Thrust of the main propeller in hover is a nonlinear (although quadratic) function of rotational speed. It can be linearized at the rotational speed required for hover, which yields a following result.

$$\Delta T = \rho(\omega_0 R)(\pi R^2) C_T R \Delta\omega \tag{3.15}$$

To cause a rolling motion, one propeller must decrease it's thrust, and the other must increase it, which also applies to rotational speed ω. Since the furthest propellers are used, the lever distance is equal to half the wingspan. That results in the following linearized acceleration equation.

$$\dot{p}_t = \frac{b}{2I_x}(2\Delta T) \tag{3.16}$$

$$= \frac{b}{I_x} \rho \omega_0 \pi R^4 C_T \Delta\omega \tag{3.17}$$

The rotational speed has to change gradually, therefore a first order system can be used for the delays, which can be chosen one order above the thruster's delays. So the whole system takes following form, with the change in rotational speed as input.

$$G_p = \frac{\frac{b}{I_x} \rho \pi R^4 C_T}{s\tau + 1} \tag{3.18}$$

The maximum control deviation $\Delta\omega$ should have a limit, which was chosen at 20 $\frac{rad}{s} = 190.99\ RPM$ That gives a maximum acceleration of $\dot{p}_t = 20.53\ \frac{m}{s^2}$, which is around four times the thruster's.

3.2.4 The complete model

Joining all the subsystems together creates the simulation roll axis model of the modelled eVTOL.

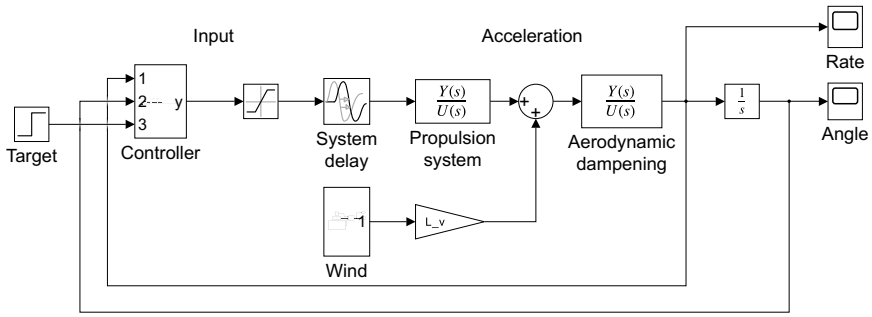

Figure 3.4: Schematic of the roll axis model

Chapter 4

Control system design and evaluation

After creating the simulation model of eVTOL's roll axis, it is possible to design and evaluate controllers and compare them to the theoretical results from before.

First, classical controllers will be evaluated, a combination of the PID variety. Later, more modern methods will be evaluated, such as switching methods, sliding mode and MPC.

Propulsion	Stabilized variable	Rise time	Step error	Stabilization time
Thruster	Rate	0.3188 s	-0.1238 $\frac{rad}{s}$	0.1371 s
	Angle	1.0354 s	-0.0085 rad	0.2267 s
Propeller	Rate	0.1487 s	-0.1238 $\frac{rad}{s}$	0.1064 s
	Angle	0.5414 s	-0.0066 rad	0.1423 s

Table 4.1: Expected theoretical results

All the controllers were tested using a MATLAB script, which gave the relevant values. For the specified variable, rate or angle, a step function was tested and then the three wind scenarios. The tolerance for settling values was 0.01 rad for angles or 0.01 $\frac{rad}{s}$ for rates.

4.1 PID controller

Root locus can be used to determine the desired location of poles and zeros. Two of the poles are well-known from the simulation model's elements. First comes from the propulsion's first order delay at position equal to $-\frac{1}{\tau}$. The other is from the aerodynamic dampening at position equal to L_P. The poles of the system delay τ_0 are problematic, as they cannot be expressed exactly, only by Padé's approximation with the rest of the system.

A cascade control structure can be used for the angular control, by utilizing the previous design for rate control, and analysing the model with the rate controller as a whole.

The design rules are to keep the system stable, i.e. the placement of the poles must stay on the negative part of the real axis. Then, mitigate the poles closest to the imaginary axis if possible. Next, to have less than 20% overshoot with a unit step response and keep the controller output within the limits for the type of propulsion and to minimize rise time.

4.1.1 Rate

With both the types of propulsion a PIDF controller was utilized. The rate controller needs to incorporate an integrator, as there is no other directly in the system, to ensure no static error [Pra00].

First, the two available zeros were placed to mitigate the poles of the propulsion and aerodynamic dampening. Then the filtration pole and gain of the controller were adjusted, so the system remains stable, and overshoot and output limits are met.

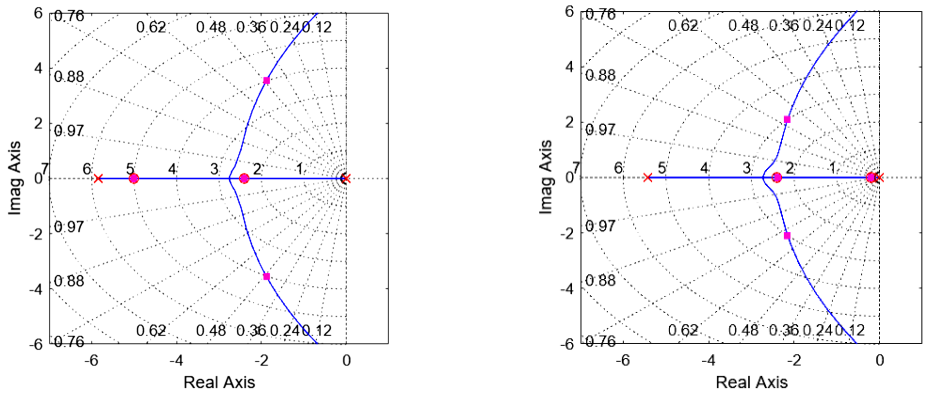

(a) : Thruster with $\tau = 0.2s$ **(b) :** Propeller with $\tau = 5s$

Figure 4.1: Root locus examples

Propulsion	Delay τ $[s]$	Rise time $[s]$	Settling time $[s]$	Wind 1 error $[\frac{rad}{s}]$	Wind 2 error $[\frac{rad}{s}]$	Wind 3 error $[\frac{rad}{s}]$	Stabilization time $[s]$
Thruster	0.2	0.670	2.87	0.0133	0.0262	-0.2653	2.33
	0.3	0.76	3.67	0.0133	0.0268	-0.2820	2.96
	0.4	0.88	3.98	0.0168	0.0334	-0.2970	3.26
	0.5	0.97	4.41	0.0182	-0.0370	-0.3083	3.62
Propeller	2	1.12	4.11	0.0224	-0.0436	-0.3221	4.29
	3	1.17	4.28	0.0229	-0.0457	-0.3262	4.42
	4	1.18	4.32	0.0228	-0.0461	-0.3272	4.44
	5	1.20	4.37	-0.0230	-0.0470	-0.3285	4.46

Table 4.2: Results for the rate PIDF controller

4.1.2 Angle

The controller for the angle is one layer above the rate controller. It sets the target rate for the rate controller, according to angular error.

There is one integrator already in the system, so it does not need to be incorporated in the controller. The closest poles to the imaginary axis are a complex pair, which cause oscillation. Mitigation of this pair is not possible with a regular PID (or similar) controller. If the next closest pole is covered with a zero from the controller, it influences the position of the complex pair, and the oscillation increases. The only PDF controller configuration that would seemingly decrease the oscillation has negative derivative coefficient, which would likely cause instability in other cases. Therefore, a P controller

was chosen.

Propulsion	Delay τ $[s]$	Rise time $[s]$	Settling time $[s]$	Wind 1 error $[rad]$	Wind 2 error $[rad]$	Wind 3 error $[rad]$	Stabilization time $[s]$
Thruster	0.2	1.25	4.98	0.0098	0.0189	-0.1413	3.30
	0.3	1.30	12.13	-0.0098	0.0192	-0.1626	7.98
	0.4	1.49	8.53	-0.0153	-0.0297	-0.1956	6.47
	0.5	1.62	9.58	0.0181	-0.0363	-0.2200	7.38
Propeller	2	1.81	10.83	0.0243	-0.0477	-0.2538	8.48
	3	1.89	10.06	0.0261	-0.0523	-0.2658	8.88
	4	1.93	10.16	0.0266	-0.0536	-0.2690	8.98
	5	1.97	10.26	-0.0274	-0.0557	-0.2737	9.07

Table 4.3: Results for the angle P and PIDF cascaded controllers

4.2 Switching and Sliding Mode controllers

Switching controller

The simplest example of a switching controller is a bang-bang controller. In theory, it is the optimal solution for some scenarios, as seen in the analytical chapter, but with real applications that is not the case.

First problem is the switching frequency, which may be unachievable with certain actuators. This can be partially solved with hysteresis for slow processes. The next problem is with delay, as the controller can cause oscillation around the target value. This is the case, that makes it unusable as a rate controller. Lastly, the controller is very sensitive to any disturbance, and in the case of angular control, it makes overreactions and therefore oscillates.

This makes the switching controllers of this kind unsuitable for this task, as even a PID controller with pulse width modulation would likely be more suitable as a controller.

Sliding mode controller

A sliding mode controller is a non-linear controller, that aims to move the variables of the system toward and across a sliding surface [Inc24]. The control law is designed using a sliding mode function and other system states.

A switching is often used with the sliding function for robustness against disturbance. Alternatively with quasi-sliding mode, a saturated high gain function can be also used, as it reduces "chattering" and is more robust against delays. Additionally, proportional parts are used for improving the steady state error and response times.

4.2.1 Rate

For rate control, the error $e[\frac{rad}{s}]$, current target rate $p_t[\frac{rad}{s}]$ and wind speed of the disturbance $v[\frac{m}{s}]$ can be taken into account. Using a combination of them, a control law can be designed.

$$u = sat(A \cdot e) - \frac{C_p}{a_t} p_t - \frac{C_v}{a_t} v \tag{4.1}$$

The gain A is the highest value, that does not overshoot by more than 15% with a unit step change. Other parameters were obtained from the model, resembling feed-forward control, so they reduce the steady state error. The problem with this approach is that the parameters need to be exact. Alternatively, this could be replaced or complemented with an integrator to achieve similar result.

Propulsion	Delay τ $[s]$	Rise time $[s]$	Settling time $[s]$	Wind 1 error $[\frac{rad}{s}]$	Wind 2 error $[\frac{rad}{s}]$	Wind 3 error $[\frac{rad}{s}]$	Stabilization time $[s]$
Thruster	0.2	0.64	1.79	-0.0043	-0.0087	-0.1736	1.18
	0.3	0.74	2.15	0.0060	-0.0121	-0.1931	1.45
	0.4	0.83	2.41	-0.0071	0.0144	-0.2075	1.62
	0.5	0.92	2.61	0.0079	0.0160	-0.2181	2.29
Propeller	2	1.14	3.83	0.0182	-0.0379	-0.2920	2.87
	3	1.22	4.08	-0.0205	-0.0429	-0.3060	3.08
	4	1.23	4.18	-0.0213	-0.0446	-0.3123	3.14
	5	1.29	4.31	-0.0227	-0.0476	-0.3188	3.27

Table 4.4: Results for the rate Sliding mode controller

4.2.2 Angle

Higher order sliding mode controllers include derivatives of the controlled variable. In this case the current roll rate $p[\frac{rad}{s}]$ can be utilized as such. For angular control, the error $e[rad]$, current rate p and disturbance wind speed $v[\frac{m}{s}]$ can be used to design a control law.

$$u = sat(A \cdot e - k \cdot p) + \frac{-C_v}{a_t} v \tag{4.2}$$

The gain A was taken from the rate controller, and the k gain was modified to dampen the system to maximum 15% overshoot during a unit step change in target. Same approach was taken with the rest of the parameters.

Propulsion	Delay τ $[s]$	Rise time $[s]$	Settling time $[s]$	Wind 1 error $[rad]$	Wind 2 error $[rad]$	Wind 3 error $[rad]$	Stabilization time $[s]$
Thruster	0.2	1.47	4.50	-0.0067	-0.0141	-0.0898	3.03
	0.3	1.62	4.85	-0.0095	-0.0200	-0.1154	3.44
	0.4	1.67	4.81	-0.0110	-0.0230	-0.1314	3.50
	0.5	1.68	4.68	0.0116	-0.0242	-0.1415	3.40
Propeller	2	2.02	7.01	-0.0232	-0.0482	-0.2325	5.80
	3	2.03	8.35	-0.0245	-0.0510	-0.2457	7.10
	4	2.01	8.41	-0.0243	-0.0504	-0.2482	7.21
	5	2.20	7.71	0.0302	-0.0633	-0.2783	7.73

Table 4.5: Results for the angle Sliding mode controller

4.3 Model Predictive Control

The Model Predictive Controller holds an internal model of the controlled system, and uses it to predict the reaction of the system to inputs and errors. It compares the predictions to the real response and acts to regulate it accordingly. This is done within fixed time steps, and the prediction is done a certain number of steps ahead.

The time step for the controllers was set to 0.1 s as that is the overall fixed delay τ_0 of the system. For the rate controller a prediction horizon of 10 and a control horizon of 5 was chosen. In case of angular control the horizons were doubled.

The controllers were designed using the MPC Designer from MATLAB, and the internal model was directly linearized from the simulation model.

Propulsion	Delay τ $[s]$	Rise time $[s]$	Settling time $[s]$	Wind 1 error $[\frac{rad}{s}]$	Wind 2 error $[\frac{rad}{s}]$	Wind 3 error $[\frac{rad}{s}]$	Stabilization time $[s]$
Thruster	0.2	0.71	3.18	0.0045	0.0149	-0.1948	1.78
	0.3	0.82	3.37	0.0062	0.0186	-0.2160	2.01
	0.4	0.93	3.56	0.0077	0.0217	-0.2309	2.21
	0.5	1.03	2.47	0.0092	0.0247	-0.2434	2.39
Propeller	2	0.83	3.12	0.0060	0.0186	-0.2230	2.68
	3	1.00	3.16	0.0086	0.0240	-0.2457	2.72
	4	1.22	3.11	0.0120	0.0315	-0.2709	3.00
	5	1.35	3.16	0.0143	0.0371	-0.2929	3.15

Table 4.6: Results for the rate MPC

Propulsion	Delay τ $[s]$	Rise time $[s]$	Settling time $[s]$	Wind 1 error $[rad]$	Wind 2 error $[rad]$	Wind 3 error $[rad]$	Stabilization time $[s]$
Thruster	0.2	1.46	4.43	0.0123	-0.0249	-0.1175	2.05
	0.3	1.55	4.69	0.0138	-0.0281	-0.1328	3.28
	0.4	1.64	4.94	0.0151	-0.0312	-0.1462	3.55
	0.5	1.73	5.16	0.0165	-0.0343	-0.1584	3.78
Propeller	2	1.66	6.39	0.0094	0.0361	-0.1649	4.80
	3	1.69	5.71	0.0271	-0.0416	-0.1654	5.06
	4	1.85	4.82	0.0231	0.0452	-0.1938	3.57
	5	2.04	7.02	0.0407	-0.0582	-0.2200	6.62

Table 4.7: Results for the angle MPC

4.4 Results

The rate and angle step response examples show that with as much as four times the control authority, the propeller as stabilization is still slower to reach the target value, due to the higher first order delay. In both scenarios the rise time increases steadily with the propulsion time constant. This shows that the delay characteristic of the propulsion is important, after a certain threshold more than the available thrust.

The wind scenarios all show the same outcome in regard to the propulsion

characteristics. The propulsion delay increases the magnitude of the error and the settling time. Even though there are two outliers, in the step disturbance stabilization times, the overall trend of the delay's influence is still prevalent.

The theoretical results are not a good estimation, but are all lower than the simulation results, which was expected, due to the added aerodynamic dampening and propulsion dynamics. Even though the estimates do not match, the principles of the importance of the delay characteristics from the analytical equation still apply.

To compare the performance of the controllers, the PID based controllers struggled with fast changing disturbances, due to a lack of feed-forward portion. The Sliding mode controllers were adequate in all cases, but proved well with rate control using the thruster. Overall best, but the most complex were the Model predictive controllers, which excelled with angular control, and usually had shorter settling times with step responses. The results produced by all controllers were similar in nature.

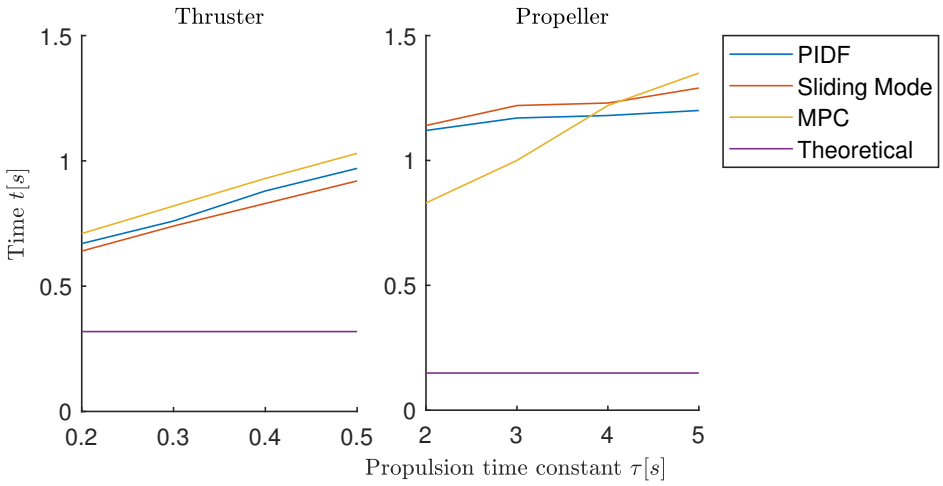

Figure 4.2: Comparison for rate control

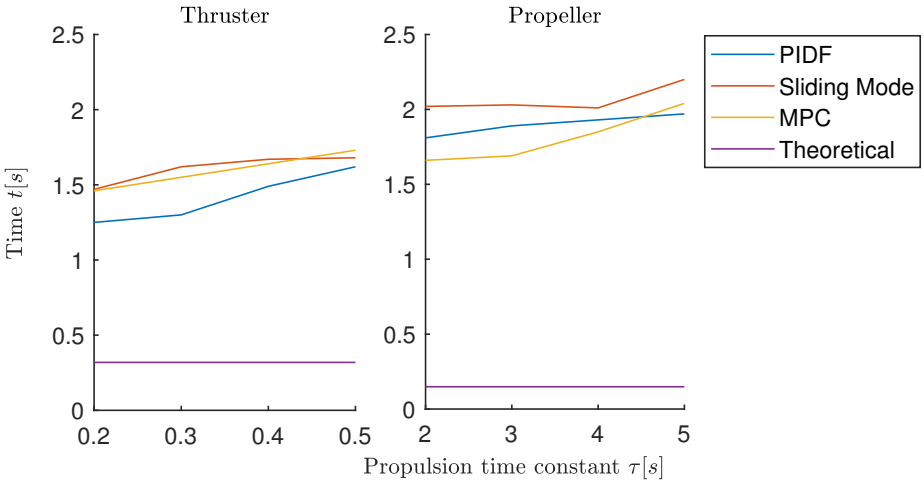

Figure 4.3: Comparison for angle control

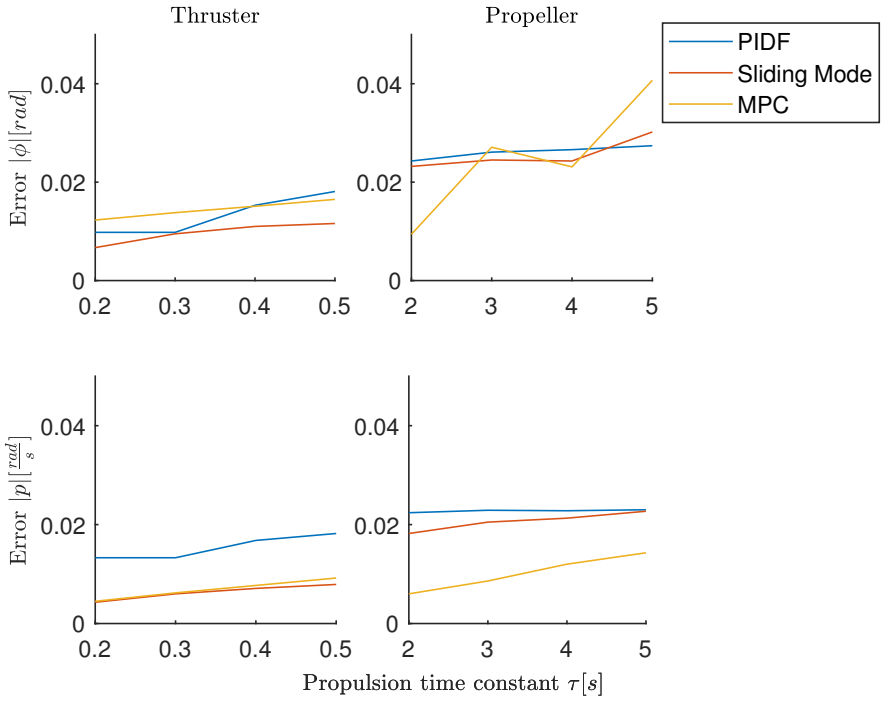

Figure 4.4: Comparison for wind 1 scenario stabilization

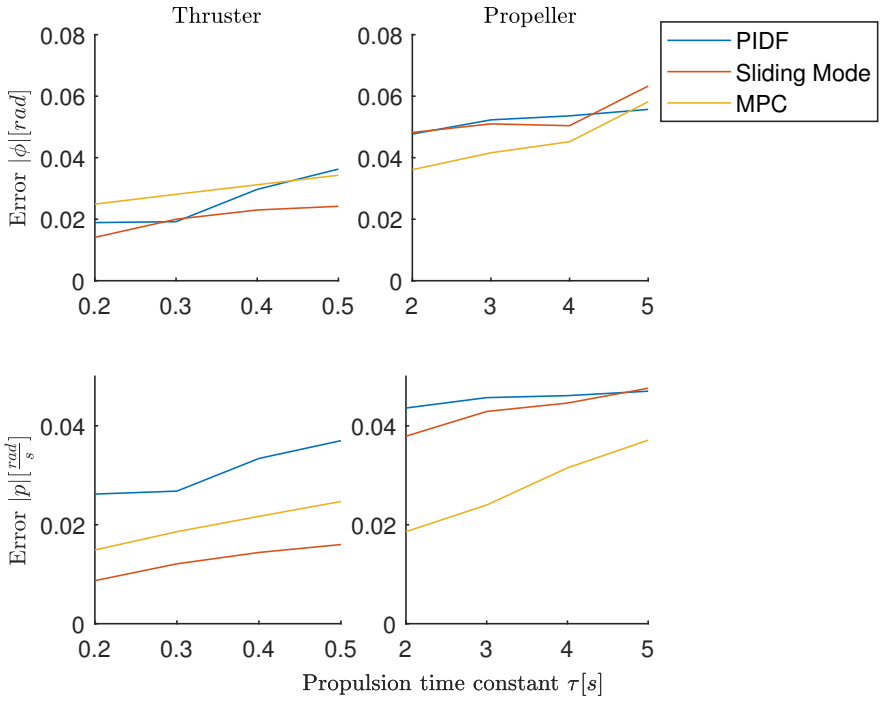

Figure 4.5: Comparison for wind 2 scenario stabilization

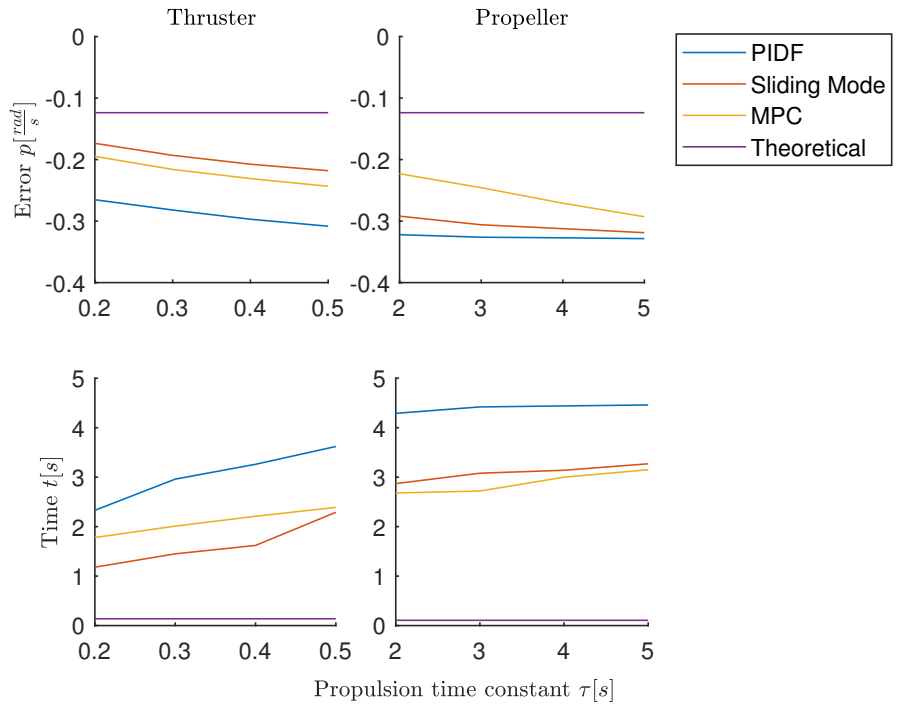

Figure 4.6: Comparison for rate wind scenario 3 stabilization

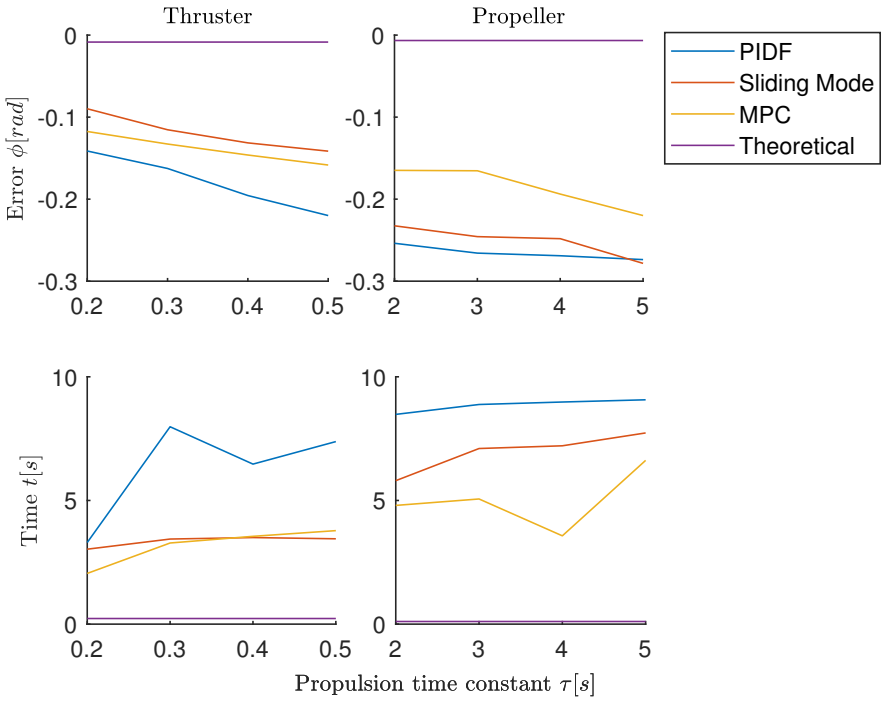

Figure 4.7: Comparison for angular wind scenario 3 stabilization

Chapter 5

Conclusion

Both analytical terms and simulation results confirm, that alternative stabilization methods, such as cold gas thrusters, could be beneficial for eVTOL vehicle stabilization. This is dependent on the vehicle itself and the propulsion already used.

Analytical terms have been formulated for minimal theoretical rise times, error magnitudes and settling times, as a function of fixed delay, available acceleration for control and acceleration caused by the disturbance. They proved accurate in the behaviour predictions, but failed in the predictions of exact values, due to the differences between the analytical and realistic scenarios.

A model eVTOL aircraft was modelled and its aerodynamic properties have been analysed, including moment stability analysis and comparison of the dimensionless aerodynamic stability derivatives to real aircraft. A set of conditions was created including changing wind conditions. Two types of propulsion have been evaluated, a quick reacting thruster and a slower propeller with higher thrust. A roll axis simulation model was then created from the gathered information.

Three control methods were designed and analysed. First a classical PIDF controller, using root locus and pole analysis. Later, more modern methods such as Sliding mode and Model predictive control, which proved more effective. The simulation results confirmed the influence of the propulsion characteristics on the stabilization performance.

5.1 Future work

The analytical portion could be expanded further to better evaluate the delay caused by the propulsion systems, for the purpose of obtaining more accurate estimate values.

The model could be evaluated on all axis, with a more complete simulation model.

5.2 Summary

For eVTOL vehicle control and stabilization, in terms of propulsion, delay characteristics are as important as the amount of thrust available. Therefore, alternative sets of propulsion could be recommended for VTOL configurations of eVTOL vehicles, as addition to slowly reacting main propulsion elements.

Appendix A

Bibliography

[52"14] "FOX 52", 2014, https://commons.wikimedia.org/wiki/File:MV-22_mcas_Miramar_2014.JPG.

[Cau11] D. A. Caughey, *Dynamics of flight vehicles*, 2011, https://courses.cit.cornell.edu/mae5070/.

[Cel19] Marek Cel, *Cessna 172 Flight Simulation Data*, 2019, doi:10.13140/RG.2.2.27040.51205, https://www.researchgate.net/publication/353752543_Cessna_172_Flight_Simulation_Data.

[DMH12] Frank D. Quinn Daniel M. Hauser, *Simulation of a Cold Gas Thruster System and Test Data Correlation*, Tech. report, NASA, Glenn Research Center, Cleveland, Ohio, 2012, https://ntrs.nasa.gov/api/citations/20120003741/downloads/20120003741.pdf.

[Dom04] Burkhard Domke, 2004, https://b-domke.de/AviationImages/Harrier/8425.html.

[Fra02] James A. Franklin, *Dynamics, Control, and Flying Qualities of V/STOL Aircraft*, American Institute of Aeronautics and Astronautics (AIAA), 2002, https://app.knovel.com/hotlink/toc/id:kpDCFQVST2/dynamics-control-flying/dynamics-control-flying.

[Hun23] Harlan Huntington, 2023, https://commons.wikimedia.org/wiki/File:Joby_Aviation_S4_experimental_eVTOL_aircraft_at_Edwards_AFB.jpg.

[Inc24] The MathWorks Inc., *Sliding Mode Control Design for Mass-Spring-Damper System*, 2024, https://uk.mathworks.com/help/slcontrol/ug/sliding-mode-control-design-for-mass-spring-damper-system.html.

[Joh13] Wayne. Johnson, *Rotorcraft Aeromechanics*, Cambridge University Press, 2013, https://ebookcentral.proquest.com/lib/cvut/detail.action?docID=1139714.

[Lea08] Frank B. Leahy, *Discrete Gust Model for Launch Vehicle Assessments*, 2008, https://ams.confex.com/ams/presview.cgi?username=129833&password=129833&uploadid=7813.

[LL57] Walter H Leisher L, *Stability derivatives of Cessna aircraft*, Tech. report, Cessna Aircraft Company, 1957.

[McC79] Barnes W. McCormick, *Aerodynamics, Aeronautics, and Flight Mechanics*, John Wiley & Sons, Incorporated, 1979.

[NTB19] U.S. Navy photo by Mass Communication Specialist 3rd Class Nathan T. Beard, 2019, https://commons.wikimedia.org/wiki/File:F-35B_Lightning_II_lands_aboard_HMS_Queen_Elizabeth_(R08)_on_17_October_2019_(191017-N-QI061-1159).jpg.

[Pin08] Adrian Pingstone, 2008, https://commons.wikimedia.org/wiki/File:BAe_Harrier_GR9_ZG502_landing_arp.jpg.

[Pra00] Roger W. Pratt, *Flight Control Systems - Practical Issues in Design and Implementation*, Institution of Engineering and Technology (The IET), 2000, https://app.knovel.com/hotlink/toc/id:kpFCSPIDI2/flight-control-systems/flight-control-systems.

[RKH72] Wayne F. Jewell Robert K. Heffney, *Aircraft handling qualities data*, Tech. report, National Aeronautics and Space Administration, 1972, https://www.roberthefley.com/docs/Data/NASA%20CR-2144--Heffley--Aircraft%20Handling%20Qualities%20Data.pdf.

[SE] Zuri.com SE, https://zuri.com/.

[Ste15] et al. Stevens, Brian L., *Aircraft Control and Simulation : Dynamics, Controls design, and Autonomous Systems*, John Wiley & Sons, Incorporated, 2015, https://ebookcentral.proquest.com/lib/cvut/detail.action?docID=4039442.

["To08] "Tosaka", 2008, https://commons.wikimedia.org/wiki/File:F-35B_Joint_Strike_Fighter_(thrust_vectoring_nozzle_and_lift_fan).PNG.